Spring 2010

# Development of a high-resolution two-dimensional urban/rural flood simulation

Jesse Alex Piotrowski
*University of Iowa*

# DEVELOPMENT OF A HIGH-RESOLUTION TWO-DIMENSIONAL URBAN/RURAL FLOOD SIMULATION

by

Jesse Alex Piotrowski

A thesis submitted in partial fulfillment
of the requirements for the
Master of Science degree in
Civil and Environmental Engineering
in the Graduate College of
The University of Iowa

May 2010

Thesis Supervisors: Professor Larry J. Weber
Adjunct Associate Professor Nathan C. Young

Graduate College
The University of Iowa
Iowa City, Iowa

CERTIFICATE OF APPROVAL

MASTER'S THESIS

This is to certify that the master's thesis of

Jesse Alex Piotrowski

has been approved by the Examining Committee for the thesis requirement for the Master of Science degree in Civil and Environmental Engineering at the May 2010 graduation.

Thesis Committee: _____
Larry J. Weber, Thesis Supervisor

_____
Nathan C. Young, Thesis Supervisor

_____
Witold F. Krajewski

To my father

Experience: that most brutal of teachers. But you learn, my God do you learn.

C. S. Lewis

ACKNOWLEDGEMENTS

First and foremost, I want to acknowledge the grace of God, Who has blessed me in so many ways during the course of my research. I thank my father and mother, who have provided immeasurable support of my education and professional career. Their guidance and sacrifice are responsible for my academic achievement. I thank Drs. Larry Weber and Nathan Young for guidance during my time at the University of Iowa; I consider them both to be mentors and friends. Nate painstakingly provided constant teaching of the various methods I used to complete this project. My thesis committee helped me focus and perfect my study and I certainly appreciate their help. I want to thank the students and support staff at IIHR – Hydroscience & Engineering for their assistance. Notably, Pete Haug and Andy Craig helped me collect hydrographic data; Bo Chen and Radek Goska developed the algorithm to extract inundation depth from the LiDAR data; Dan Gilles and Nathan Quarderer helped me with numerical modeling and geospatial techniques; Brian Miller and Mark Wilson provided constant hardware and software support; and Mike Kundert helped with visual design of my simulation outputs. The University of Iowa provided topographic data and the one-dimensional model, generated under contract by Ayres Associates. Dusty Robinson of Ayres Associates provided information on a regular basis and I appreciate his assistance.

ABSTRACT

Numerical modeling of extreme flooding in an urban area in eastern Iowa is presented. Modeling is performed using SRH-2D, an unstructured grid, finite volume model that solves the depth-averaged shallow-water equations. Data from a photogrammetric stereo compilation, contour maps, a hydrographic survey and building records were used to create a digital elevation model depicting the river channel and floodplain. A spatially distributed Manning coefficient based on land cover classification, derived from aerial photography is also used. The model is calibrated with high-resolution inundation depth data derived from a 1 m light detection and ranging survey, collected during the falling limb of the flood hydrograph, and discrete global positioning system measurements of water surface elevation at a bankfull condition. The model is validated with discrete high water marks collected immediately after the flood event. Results show the model adequately represents the water surface elevation in the main channel and floodplain and that exclusion of the discharges from minor creeks did not affect simulation accuracy. Reach scale results are not affected by the presence of buildings, but local inconsistencies occur in shallow water if buildings are not removed from the mesh. An unsteady hydrograph approximates flood hydrodynamics better than a steady-state simulation, but extreme computation time is not feasible for most investigations. The two-dimensional model is compared to a comparable one-dimensional model of the study reach. The 1D model suffers an inability to accurately predict inundation depth throughout the entire study area.

TABLE OF CONTENTS

LIST OF TABLES

LIST OF FIGURES

# CHAPTER 1: INTRODUCTION

In June of 2008, eastern Iowa experienced significant flooding on numerous rivers which affected the lives of thousands of individuals. One community particularly affected by the flood was Iowa City, the home of The University of Iowa. Iowa City is located along the Iowa River approximately 8 miles downstream of the United States Army Corps of Engineers (USACE) Coralville Lake flood control project. Heavy winter snows and spring rainfall led to saturated soil conditions in the Iowa River catchment. Excessive rainfall in the Iowa River catchment during the middle of June filled Coralville Lake, resulting in uncontrolled release from its emergency spillway. Excessive outflow from Coralville Lake created an event in Iowa City and the adjacent community of Coralville that exceeded the 500 year probability, as defined by the Federal Emergency Management Agency (FEMA). The flood inundated numerous homes, businesses, and public properties, put several bridges and utilities at severe risk, and caused hundreds of millions of dollars in damage.

The objective of the present study is to develop a high-resolution, two-dimensional (2D), depth-averaged numerical model of a 10-mile reach of the Iowa River corridor, beginning at the Coralville Lake outlet and extending south to the southern corporate limit of Iowa City. Other objectives include comparing the accuracy and efficiency of one-dimensional (1D) and 2D hydraulic models, validating the assumption that steady-state discharge can approximate an unsteady condition, quantifying the effect of minor creek discharges and comparing a common method of representing buildings in the floodplain to removal of buildings from flow computations.

To simulate flow in the Iowa River corridor, bathymetric, topographic, and hydrographic data were used in conjunction with the United States Bureau of Reclamation (USBR) Sedimentation and River Hydraulic Two-Dimensional (SRH-2D) software to generate a 2D depth-averaged hydraulic model. The model was validated using an aerial Light Detection and Ranging (LiDAR) survey conducted during the

falling peak of the 2008 flood hydrograph. Hydrodynamic simulations will be used to create a library of high-resolution maps along the Iowa River corridor, identifying the extent of flood inundation and magnitude of velocity associated with river flow and stage data reported by the National Weather Service. These maps will allow the local community agencies and citizens to better understand their individual flood risks, make more informed decisions about flood mitigation alternatives, and take appropriate actions to ensure safety and reduce damage during flood events. Maps of inundation depth and depth-averaged magnitude of velocity will also help anticipate localized flood hazard zones where high depth or dangerous velocity is likely to occur.

# CHAPTER 2: LITERATURE REVIEW

In recent years the cost-effective generation of spatially-distributed numerical river corridor models has been facilitated by advances in numerical model development, enhanced remote sensing and increased computing power. The proliferation of high-resolution digital elevation maps, hydrographic data and constant development of numerical tools has resulted in the development of hydrodynamic models capable of producing quantitative assessments of flood risk at very fine spatial and temporal scales. However, an increase in model resolution does not necessarily indicate a proportional decrease in uncertainty. Thus the required resolution and dimensionality of hydrodynamic models must be considered for each individual case (Hunter, et al. 2007).

## 2.1 Types of numerical hydraulic models

Hydraulic models are classified according to the number of dimensions in which they represent the spatial domain. The selection of a one-, two- or three-dimensional model depends on the complexity of the flow processes to be numerically simulated. Out-of-bank flow in meandering compound channels, like that considered in the present study, is known to be highly three-dimensional, involving a strong shear layer between main channel and floodplain flows (Bates and Roo 2000). The three-dimensional flow field is described by continuity. The continuity equation, presented as Equation 2.1, can be used to derive the Navier-Stokes equations for an incompressible (or Newtonian) fluid. The Navier-Stokes equations, which describe the velocity field within a fluid, are presented as Equations 2.2 through 2.4. These three equations represent the basis for all hydrodynamic simulation. Various simplifications can be made to the equations based on the characteristics of the flow conditions simulated.

$$\frac{\partial p}{\partial t}+\frac{\partial u}{\partial x}+\frac{\partial v}{\partial y}+\frac{\partial w}{\partial z}=0 \tag{2.1}$$

$$\rho\left(\frac{\partial u}{\partial t}+u\frac{\partial u}{\partial x}+v\frac{\partial u}{\partial y}+w\frac{\partial u}{\partial z}\right)=-\frac{\partial p}{\partial x}+\mu\left(\frac{\partial^2 u}{\partial x^2}+\frac{\partial^2 u}{\partial y^2}+\frac{\partial^2 u}{\partial z^2}\right)+\rho g_x \tag{2.2}$$

$$\rho\left(\frac{\partial v}{\partial t}+u\frac{\partial v}{\partial x}+v\frac{\partial v}{\partial y}+w\frac{\partial v}{\partial z}\right)=-\frac{\partial p}{\partial y}+\mu\left(\frac{\partial^2 v}{\partial x^2}+\frac{\partial^2 v}{\partial y^2}+\frac{\partial^2 v}{\partial z^2}\right)+\rho g_y \tag{2.3}$$

$$\rho\left(\frac{\partial w}{\partial t}+u\frac{\partial w}{\partial x}+v\frac{\partial w}{\partial y}+w\frac{\partial w}{\partial z}\right)=-\frac{\partial p}{\partial z}+\mu\left(\frac{\partial^2 w}{\partial x^2}+\frac{\partial^2 w}{\partial y^2}+\frac{\partial^2 w}{\partial z^2}\right)+\rho g_z \tag{2.4}$$

In the equations above, $\rho$ is water density, $t$ is time, $x$, $y$ and $z$ are Cartesian coordinates, $u$, $v$ and $w$ are velocity components in the $x$, $y$ and $z$ directions, respectively, $p$ is pressure, $\mu$ is viscosity and $g$ is gravitational acceleration. Because of the complexity of the equations, application of fully three-dimensional numerical schemes at reach scale (5 – 50 km) is not practical when a simpler numerical scheme can adequately predict parameters of interest (velocity direction and magnitude, inundation extent, and water depth) (Bates and Roo 2000).

Until relatively recently, 1D finite difference solutions of the Navier-Stokes equations such as those employed by MIKE11 and HEC-RAS software have been the most popular approach to estimate flood inundation (Bates and Roo 2000). These software use a series of cross-sections oriented perpendicular to the primary flow direction to describe the river channel and floodplain. All simulated values (depth, velocity, discharge) are cross-sectional-averaged quantities. Equation 2.5 presents a general form of the section-averaged Navier-Stokes equation.

$$\frac{\partial U_{AVG}}{\partial t}+U_{AVG}\frac{\partial U_{AVG}}{\partial x}+g\left(\frac{\partial h}{\partial x}+S_f-S_0\right)=0 \tag{2.5}$$

In the equation above, $U_{AVG}$ is section averaged velocity, $h$ is water depth, $x$ is re-defined as distance in the primary flow direction, $S_f$ is the friction slope and $S_0$ is the bed slope. One-dimensional codes are computationally efficient, but lack the ability to simulate lateral diffusion of flood waves (Hunter, et al. 2007). Furthermore, water depth and

section-averaged velocity for areas between cross-sections must be estimated from model results based on linear interpolation. Cross-section location and orientation is subjective, which creates the potential for poor model results due to modeler inexperience (Bates and Roo 2000).

## 2.2 Two-dimensional numerical models

To overcome the limitations of 1D models while maintaining practicality, 2D codes have been developed by depth-averaging, rather than section-averaging, the Navier-Stokes equations. The depth-averaged Navier-Stokes equations are referred to as the Saint-Venant shallow water equations. Two-dimensional numerical schemes can be classified as either full solutions to the shallow water equations or simplified approximations in which the inertia terms are omitted from the controlling equations (often referred to as zero-inertia schemes). Zero-inertia models are acceptable prediction tools when validation data are sparse and contain error. Neglecting inertia terms requires the assumption that flow over inundated areas is a slow, shallow phenomenon. Zero-inertia schemes can justify this assumption and provide results that are accurate at the reach scale, but local inaccuracies will occur (Hunter, et al. 2007).

Because the purpose of the current investigation is to provide accurate inundation data at the local scale, a numerical model that solves the full, dynamic Saint-Venant equations was required. Equations 2.6 through 2.8 list the Saint-Venant equations. Equation 2.6 represents continuity and Equations 2.7 and 2.8 describe conservation of momentum in the fluid.

$$\frac{\partial h}{\partial t}+\frac{\partial (hU)}{\partial x}+\frac{\partial (hU)}{\partial y}=0 \tag{2.6}$$

$$\frac{\partial (hU)}{\partial t}+\frac{\partial (hUU)}{\partial x}+\frac{\partial (hVU)}{\partial y}=\frac{\partial (hT_{xx})}{\partial x}+\frac{\partial (hT_{xy})}{\partial y}-gh\frac{\partial z}{\partial x}-\frac{\tau_{hx}}{\rho} \tag{2.7}$$

$$\frac{\partial(hV)}{\partial t}+\frac{\partial(hUV)}{\partial x}+\frac{\partial(hVV)}{\partial y}=\frac{\partial(hT_{xy})}{\partial x}+\frac{\partial(hT_{yy})}{\partial y}-gh\frac{\partial z}{\partial y}-\frac{\tau_{hy}}{\rho} \tag{2.8}$$

In the equations above, $U$ and $V$ are depth-averaged velocity components in the $x$ and $y$ directions, respectively, $T_{xx}$, $T_{xy}$, and $T_{yy}$ are depth-averaged turbulent stresses, $z$ is water surface elevation (WSE) and $\tau_{hx}$, $\tau_{hy}$ are the bed shear stresses due to friction. Comparing the Navier-Stokes equations to the depth-averaged Saint-Venant equations, one can see that all horizontal velocity terms have been depth-averaged, thus removing all differential terms in the vertical direction (Lai 2009).

Determination of turbulent stresses, dispersion terms and bed shear stress is dependent on numerical model formulation. Equations 2.9 through 2.13 express the aforementioned terms as calculated by SRH-2D. Bed friction values in the $x$ and $y$ directions, respectively, are calculated using Equations 2.9 and 2.10, where $n$ is the Manning's roughness coefficient. Manning's roughness coefficient is a local constant that does not change with flow rate, but varies spatially as discussed in Chapter 4.

$$\tau_{hx}=\rho\left(\frac{gn^2}{h^{1/3}}\right)U\sqrt{U^2+V^2} \tag{2.9}$$

$$\tau_{hy}=\rho\left(\frac{gn^2}{h^{1/3}}\right)V\sqrt{U^2+V^2} \tag{2.10}$$

Depth-averaged turbulent stresses are based on the Boussinesq equations, presented in Equations 2.11 through 2.13.

$$T_{xx}=2(\nu+\nu_t)\frac{\partial U}{\partial x}-\frac{2}{3}k \tag{2.11}$$

$$T_{xy}=(\nu+\nu_t)\left(\frac{\partial U}{\partial y}+\frac{\partial V}{\partial x}\right) \tag{2.12}$$

$$T_{yy}=2(\nu+\nu_t)\frac{\partial V}{\partial y}-\frac{2}{3}k \tag{2.13}$$

In the equations above, $v$ is kinematic viscosity of water, $v_t$ is turbulent eddy viscosity, and $k$ is turbulent kinetic energy. A depth-averaged parabolic turbulence model, presented as Equation 2.14, was used to compute the turbulent eddy viscosity and all terms involving turbulent kinetic energy are neglected.

$$v_t = \alpha U_* h \tag{2.14}$$

In Equation 2.6, $U_*$ is bed frictional velocity and $\alpha$ is the parabolic turbulent model coefficient, which ranges from 0.3 to 1.0. Final results may not be sensitive to the turbulent model coefficient for most applications (Lai 2009).

## 2.3 Numerical discretization

The Saint-Venant equations have few exact solutions but numerical techniques can be used to obtain discretized results. Discretization requires selection of a computational element size ($\Delta x$) and a time step ($\Delta t$). The time derivative term may be discretized using explicit (forward-looking) or implicit (backward-looking) schemes. The two methods differ in terms of stability and complexity of the algorithms required to solve the resulting equations (Hunter, et al. 2007). Explicit schemes use quantities calculated from the previous time step ($t^{n-1}$) to compute dependent variables at the current time step ($t^n$). Explicit schemes are simple to program but require careful selection of the model time step, as it dictates the stability of the scheme. The Courant-Friedrichs-Lewy (CFL) equation must be satisfied if numerical stability is to be achieved for explicit schemes. The CFL condition is presented in Equation 2.15, where the left side of the equation is referred to as the CFL or Courant number. (Cunge, Holly and Verwey 1980).

$$\left| (gh)^{1/2} \frac{\Delta t}{\Delta x} \right| \leq 1 \tag{2.15}$$

The combination of complex topography and varying flow conditions often requires a computational time step which is very small compared to the characteristic time scales for physical phenomena (Hunter, et al. 2007).

Implicit schemes compute dependent variables using quantities from the previous time step and quantities at the current time step. A matrix or other iterative technique must be used to obtain solutions. Thus all cells within the domain are coupled in the computation process, and hydraulic effects are transmitted through the entire computational mesh. This coupling process results in increased computational cost. However, implicit schemes are unconditionally stable and allow larger time steps. Therefore, time step selection is based on physical processes within the model domain and not numerical stability. In many cases, these benefits outweigh the additional computational cost (Hunter, et al. 2007; Cunge, Holly and Verwey 1980).While stability is not affected by time step, the CFL number is a good indicator of solution quality. Values less than 5 have been successfully used with implicit schemes (Bates, et al. 1998).

Multiple options exist for spatial discretization of computational schemes. Modern GIS tools can be used to easily generate structured, rectangular grid-based models from topographic and bathymetric data. However, need for increased spatial precision may lead to large, cumbersome meshes and consequently large computational costs (Hunter, et al. 2007). Computational efficiency can be increased by using coupled numerical schemes which calculate flow in the river channel using 1D section-averaged equations and flow in the floodplain using 2D depth-averaged equations (Bates and Roo 2000). Unstructured, irregularly-shaped meshes also increase efficiency by using small mesh elements in areas of interest and larger elements in less critical areas (Lai 2009). Unstructured meshes are of particular value in urban flood simulations similar to the present effort. Coarse mesh resolution can create artificial blockages between buildings and subsequently cause inaccurate simulation predictions. Finer mesh resolution is required in the vicinity of large buildings and buildings with narrow separations to

prevent local prediction errors (Neal, et al. 2009). Street depressions must be adequately refined with multiple computational elements in cross-section to accurately predict WSE of extreme flood events in urban environments (Gallegos, Schubert and Sanders 2009).

## 2.4 Boundary conditions

Spatial discretization is closely linked to the boundary conditions required for a numerical model. Flood inundation models require topographic and bathymetric data to construct the computational mesh, spatially distributed values of flow resistance and bulk flow data. Depending upon the hydrodynamic conditions modeled, additional hydrologic data, such as precipitation, upland runoff, evapotranspiration and groundwater exchange may be necessary (Hunter, et al. 2007).

Spatial distribution of topographic and bathymetric data directly affects the accuracy and stability of numerical simulations. In urban areas, flow occurs primarily in streets and alleyways; therefore topographic data must be dense enough to resolve these features. Over-simplification of street profiles can significantly alter numerical results and cause global depth errors (Mignot, Paquier and Haider 2006). Low resolution data can also create artificial blockages between buildings in the DEM (Neal, et al. 2009). Fine mesh resolution will not prevent these errors if coarse topographic data is used to establish mesh elevations.

Some measure of bed resistance must be applied to all computational elements within the mesh domain. Roughness coefficients parameterize flow resistance and may be estimated from field observation (Chow 1959). However, methods for modeling energy loss vary by code dimensionality and physical process representation. Numerical schemes with simplifying assumptions may use an effective roughness parameter to represent additional sources of energy loss, such as loss due to channel curvature (Mason, et al. 2003). In some cases, models that simulate various bulk flow conditions may require multiple sets of calibrated parameters. To simplify calibration the most critical hydraulic condition under investigation should be used to calibrate the model (Lai and Bountry

2007). Effective roughness parameters are adjusted iteratively to optimize the fit between simulation results and observations. The required computational cost often limits roughness parameterization to a uniform floodplain value or broad estimation of the spatially heterogeneous surface (Horritt 2000). More physically consistent models provide the opportunity for investigators to explicitly calculate roughness parameters from field measurements (Hunter, et al. 2007). Recent work (Mason, et al. 2003) has used LiDAR data to establish spatiotemporally varying roughness coefficients to each computational cell. Investigators have also used a compromise of the two approaches and assigned spatially distributed roughness coefficients based on land cover (Gallegos, Schubert and Sanders 2009). Other investigations have applied different friction coefficients based on the width of the streets and obstacles with moderate success (Mignot, Paquier and Haider 2006).

Numerical models require, at minimum, flow boundary conditions at all exterior inflows and outflows. Additional, internal boundary conditions can define hydraulic sources and sinks or define water surface elevations based on established formulas (e.g. wiers, low head dams) or additional quantitative data such as rating curves (Cunge, Holly and Verwey 1980). Downstream boundary conditions are typically based on an established rating curve for a given river cross-section where a uniform flow condition can be assumed (Pappenberger, et al. 2006).

Flood inundation simulations over long river reaches may require additional data to represent the contribution of distributed hydrologic inputs, such as precipitation within the model domain, upland runoff from the surrounding catchment, evapotranspiration and groundwater exchange (Hunter, et al. 2007). Numerical models of long river reaches (up to 60km) have been validated without the use of these hydrologic data (Bates, et al. 1998). However, a model containing a long river reach or a reach that is located in the upper portion of a catchment may require consideration of these processes to maintain an acceptable level of accuracy (Hunter, et al. 2007). Thus the location and size of the

numerical model should be assessed on a case by case basis to determine whether distributed hydrological inputs should be included.

## 2.5 Sources of error

Uncertainties in simulation results are due to assumptions related to theoretical model development (simplifying assumptions and numerical discretization errors) and the input data used (uncertainty in boundary and initial conditions). For two-dimensional simulation, uncertainty related to the shallow water assumption and numerical discretization is inherent but relatively insignificant compared to uncertainty in boundary conditions (Lai and Bountry 2007).

Topographic data used to estimate floodplain geometry is often defined by low resolution (10 m or greater) DEM data. Even LiDAR data, which typically represents the best available topographic data, has limited resolution (1 m) and vertical accuracy (± 15 cm) (Mason, et al. 2003). Other, more readily available topographic data will have lower vertical precision (> 15 cm) (Schumann, et al. 2007). Lower spatial resolution results in decreased accuracy of numerical results. Cook and Merwade (2009) found that decreasing spatial resolution from 6 m to 30 m resulted in a 6 percent change in inundation area. Schumann, et al. (2007) found that a spatial resolution of 25 m and a vertical accuracy of 0.5 m is required to assess flood impacts in small (10 km), heterogeneous river reaches and resampling a low-resolution DEM will not improve simulation results.

Bathymetric data used in numerical models is typically collected using single- or multi-beam echosounder systems (SBES and MBES, respectively). Bathymetric data collected using SBES or MBES are subject to uncertainty primarily due to (1) heave, pitch and roll of the survey vessel, (2) false or inaccurate soundings due to obstructions in the water column or unconsolidated bed material, (3) uncertainty in sound velocity profile or inadequate spatial and/or temporal distribution of profiles (4) latency of system components and (5) uncertainty in sounding georeference (Huang, Zhai, et al. 2002;

Clarke, Mayer and Wells 1996). Both MBES and SBES require a global navigation satellite system (GNSS) to georeference soundings. The accuracy of the GNSS depends on the inherent precision of the system, atmospheric conditions and obstructions (i.e. bridge decks, overhanging trees). Errors in both vertical and horizontal directions can also occur due to inexact benchmark information. SBES are typically not corrected for pitch and roll of the survey vessel, while most MBES applications use Inertially-Aided Real-Time Kinematic (IARTK) corrective systems to account for the motion of the survey vessel. Accurate IARTK corrections require extensive calibrations of the entire survey system to precisely determine the offset distances and angles of the echosounder, accelerometers, and GNSS. Even with extensive calibration, calibration residuals will likely exist, causing systematic error (Huang, Zhai, et al. 2002). Uncertainty in processed MBES data can be reduced because of the high density of soundings in shallow water. Each sounding can be compared to a large number of other soundings in close proximity. Soundings that do not correctly measure depth can be identified and removed. Identification of "outliers" can be performed manually or automatically by existing algorithms (Calder and Mayer 2003). Thus data collected using MBES can be considered more accurate than SBES data if all other variables are the same.

Bulk flow boundary conditions are often based on established rating curves, which are subject to uncertainty resulting from (1) measurement error in cross-sectional geometry and velocity distribution and (2) simplifying assumptions (linearity and/or uniformity of depth and velocity between measurements). Most individual discharge measurements have standard errors ranging from 3 percent to 6 percent (Sauer and Meyer 1992). Furthermore, overbank flow invalidates the assumption of uniform flow, increasing the uncertainty bounds in the rating curve. Uncertainty in discharge can increase to approximately 20 percent for peak flow conditions (Pappenberger, et al. 2006).

Roughness values are often based on visual observation and land cover heterogeneity is not fully described due to lack of data. Uncertainty in roughness values is likely, especially if there is a lack of discharge, velocity, or WSE data to perform quantitative calibration (Lai and Bountry 2007). Furthermore, roughness values are often used as the primary calibration parameter for hydraulic models. Coupled with the fact that the same data set is often used for model calibration and validation, validation of simulations is limited by the uncertainty in model parameterizations (Mason, et al. 2003).

## 2.6 Summary

Cost-effective generation of spatially-distributed numerical river corridor models has been facilitated by advances in remote sensing and computing power. However, the required resolution and dimensionality of hydrodynamic models must be considered (Hunter, et al. 2007). While out-of-bank flow in meandering compound channels is known to be highly three-dimensional, application of fully three-dimensional numerical schemes at reach scale is rarely practical (Bates and Roo 2000). One-dimensional finite difference schemes have historically been the most popular approach to estimate flood inundation (Bates and Roo 2000). However, 1D schemes cannot be used to accurately represent small scale features and linear interpolation is required to calculate properties for areas between cross-sections (Bates and Roo 2000). To overcome the limitations of 1D models, 2D models that simulate depth-averaged parameters have been developed.

Because the purpose of the current investigation is to provide inundation data that are accurate at the local scale, SRH-2D, a numerical code that solves the full, dynamic Saint-Venant equations, was selected. SRH-2D uses an implicit numerical scheme, which is more computationally intensive than explicit schemes but is unconditionally stable and allows large time steps (Hunter, et al. 2007; Cunge, Holly and Verwey 1980). SRH-2D uses an unstructured, irregularly-shaped mesh to increase efficiency by using small mesh elements in areas of interest and larger elements in less critical areas (Lai 2009). Finer

mesh resolution is required near buildings, in narrow alleys (Neal, et al. 2009) and street depressions to accurately predict flow behavior (Gallegos, Schubert and Sanders 2009).

Flood inundation models require topographic and bathymetric data to construct the computational mesh, spatially distributed values of flow resistance and bulk flow data (Hunter, et al. 2007). Spatial resolution of topographic and bathymetric data directly affects the accuracy and stability of numerical simulations (Neal, et al. 2009). Numerical schemes often may use an effective roughness parameter to estimate flow resistance (Mason, et al. 2003), in which case the most critical hydraulic condition under investigation should be used to calibrate the model (Lai and Bountry 2007). Flow boundary conditions, typically based on established rating curves are required (Pappenberger, et al. 2006), and internal boundary conditions can define hydraulic sources and sinks or define water surface elevations (Cunge, Holly and Verwey 1980). Models of long river reaches may require additional hydrologic data, and the location and size of the numerical simulation should be assessed on a case by case basis to determine whether distributed hydrologic processes should be included (Hunter, et al. 2007).

Uncertainties in simulation results related to the shallow water assumption and numerical discretization are inherent but relatively insignificant compared to uncertainty in boundary conditions (Lai and Bountry 2007). Topographic data used for floodplain geometry are often defined by low resolution DEM data (Mason, et al. 2003). Bathymetric data collected using MBES and SBES suffer uncertainty due to the motion of the survey vessel, properties of the water column (Huang, Zhai, et al. 2002) and georeferencing errors. Bulk flow boundary conditions have standard errors ranging from 3 percent to 6 percent for less-than-bankfull flow conditions (Sauer and Meyer 1992) and up to 20 percent for out-of-bank conditions (Pappenberger, et al. 2006). While roughness is often used as the primary calibration parameter (Mason, et al. 2003), uncertainty in roughness values is likely (Lai and Bountry 2007).

# CHAPTER 3: DATA COLLECTION

## 3.1 Study location

Figure 3.1 displays the study area. The City of Iowa City is located along both the western and eastern banks of the Iowa River, a tributary of the Upper Mississippi River. The University of Iowa is partially located within the Iowa River floodplain. The City of Coralville is located along the western bank of the Iowa River and along the northern bank of Clear Creek. Both Iowa City and Coralville are located downstream of the Coralville Lake. The study area extends from the outflow of Coralville Lake south to the southern corporate limit of Iowa City. The western boundary of the study area is approximately located at the western corporate limit of Coralville and the eastern boundary is the bluffs along the Iowa River floodplain. United States Geological Survey (USGS) stream gages exists directly downstream of the outlet of Coralville Lake and on Clear Creek to the west of its confluence with the Iowa River. Two smaller creeks, Rapid and Ralston, exist in the study area as well. Rapid creek is gauged and Ralston is not gauged.

## 3.2 Overview

At the reach scale, data collection efforts include a bathymetric survey of the Iowa River channel and a high resolution Light Detection and Ranging (LiDAR) survey. Topographic data was provided by the United States Geological Survey (USGS) and the cities of Iowa City and Coralville. Ayres Associates collected and integrated topographic and aerial photogrammetric data. Global information systems (GIS) maps delineating the location of structures and plan sets for bridge piers, spillways and culverts within the study reach were obtained from the University of Iowa and the cities of Iowa City and Coralville.

## 3.3 Bathymetry

### 3.3.1 Methodology

Bathymetric data were collected to define the bed geometry in the Iowa River channel. The bathymetric survey began in July 2008 and was completed in October 2008. Bathymetric data were collected with both single- and multi-beam hydrographic survey systems. Figure 3.2 displays the extent of each survey.

Channel bed soundings along the entire study reach were collected using a single-beam echosounder deployed from an 18 foot Polarkraft tunnel hull boat. A 200 kHz Odom Hydrographic HT100 survey-grade single-beam sonar with a 3 degree transducer was used to collect individual depth measurements along transects spaced 100 ft apart, perpendicular to the direction of flow. Depth measurements were synchronized with horizontal position (latitude and longitude) and water surface elevation, measured with a Trimble R8 real-time kinetic (RTK) GNSS. The hydrographic surveying software package HYPACK 2008 was used to convert the latitude and longitude to a projected geographic coordinate system and to record the coordinates and soundings. Vertical and horizontal survey control was established using the Johnson County, Iowa GNSS control network. Elevation data from the RTK GNSS were time averaged using a moving 30 second window. Depth measurements and the vertical distance between the phase center of the RTK GNSS and the sounding surface of the echosounder were subtracted from the time-averaged elevation of the RTK GNSS to calculate river bed elevations. This calculation assumes the RTK GNSS unit was directly above the echosounder and the echosounder was oriented normal to the water surface. These two assumptions are not valid at all times, as the survey vessel experienced pitch and roll during the survey. A pitching or rolling vessel introduces error in spatial reference provided by the RTK GNSS and depth measurement. Single-beam data were filtered using HYPACK. Automatic filters were used to remove bed elevations where the RTK GNSS horizontal and/or vertical dilution of precision (HDOP, PDOP) was not within acceptable standard

survey limits (0.02 m and 0.04 m, respectively). Automatic filters were also used to remove bed elevations that deviated significantly (greater than 0.2 m) from adjacent soundings. These data were assumed to be inaccurate soundings or debris not representative of the surrounding bed elevation.

Supplemental high-resolution bathymetric data were collected over a 1.2 kilometer reach of the Iowa River adjacent to the University of Iowa campus and downtown Iowa City, during the falling limb of the 2008 flood hydrograph. Bed soundings were collected using a state-of-the-art RESON SeaBat 7125 multi-beam echosounder, simultaneously sampling 512 locations on the river bed in a 120-degree swath perpendicular to the direction of travel. An Applanix POS-MV inertial motion detection system was used to track heading, pitch, roll, and yaw of the survey vessel. Bed soundings were synchronized with a RTK GNSS. Latitude, longitude, and depth were sampled at a rate of approximately 2 Hz. HYPACK was used to convert the latitude and longitude to a projected geographic coordinate system and to record the coordinates and soundings. Vertical and horizontal survey control was established using the Johnson County, Iowa GNSS control network. Elevation data from the RTK GNSS were time averaged using a moving 30 second window. HYPACK automatically calculated bed elevation for each depth sounding by applying the corresponding time averaged elevation data and pitch, roll, and yaw values. Multi-beam data were filtered using HYPACK. Automatic filters were used to remove bed elevations that deviated from the adjacent soundings. Mean elevation values were used where data overlap occurred. When the multi-beam system was used beneath bridges automatic filters could not remove bed elevations where the HDOP and PDOP were not within acceptable standard survey limits. However, the RTK GNSS and the inertial motion detection system were used to estimate boat position and heading when RTK signal was lost directly beneath bridge decks. Multi-beam data density was reduced in HYPACK and interpolated to a grid with

a constant horizontal cell spacing of 20 cm. The mean elevation within each cell was applied at the cell center.

### 3.3.2 Measurement uncertainty and comparison

Table 3.1 lists uncertainty values for the various pieces of equipment used to collect single- and multi-beam data. Rigorous uncertainty and precision analysis was not conducted for the hydrographic surveys. However, single- and multi-beam data sets were compared to evaluate the accuracy and repeatability of the bathymetric surveys. Both data sets were exported from HYPACK as discrete points with X, Y, Z coordinates. ArcGIS was used to compare data where overlap occurred. The multi-beam data, exported as a grid of points with a constant horizontal cell spacing of 20 cm, was converted to a raster with a cell size of 20 cm. The raster pixel values represented the Z values of the multi-beam data. The single-beam data was also converted to a raster with a cell size of 20 cm and pixel values equal to the Z values of the single-beam points. The single-beam raster was subtracted from the multi-beam raster where the datasets intersected. Figure 3.3 displays a histogram of elevation difference between single- and multi-beam data. The majority of differences were within the range -0.25 m to 0.15 m. Because the single- and multi-beam surveys were performed at different times, the difference in bed elevation can be attributed to actual change in the river bed as well as error in the bathymetric surveys.

The two datasets were combined to create a single continous dataset. To prevent minor discontinuities in the bed elevation, the single-beam data were not included where multi-beam and single-beam data overlapped. To ensure a smooth transition between multi-beam and single-beam data, the multi-beam raster was converted to a polygon in ArcGIS and a 1 m buffer was applied. All single-beam data within this zone was deleted. Figure 3.4 displays treatment of the overlapping datasets.

## 3.4 Topography

Topographic data for the study area were acquired from Ayres Associates, the City of Iowa City, the City of Coralville and the USGS. The Cities of Iowa City and Coralville provided 2-foot contour maps obtained in 2006 for most of the project area. Coarser 10-foot contour maps of the northern portion of the study reach were obtained from the USGS. Ayres Associates acquired a 1/2-foot contour map from a photogrammetric stereo compilation conducted in November, 2008, for a large portion of the study area. Ayres Associates provided a digital terrain model (DTM) that compiled the topographic data within the study area. When overlap of data sets occurred, the highest resolution data were used.

## 3.5 Digital elevation model

The DTM provided by Ayres Associates was used as the basis for the hydraulic model. The DTM was modified to create a digital elevation model (DEM). Bathymetry data were added to describe the geometry of the Iowa River channel. Two low head dams and twelve major bridges along the Iowa River were added. Multiple culverts along Ralston Creek required modification. Thousands of residential, commercial, and industrial buildings within the study area were added as well. Figure 3.5 displays the features added to create the DEM.

### 3.5.1 Inclusion of low head dams

Two low head dams exist along the Iowa River within the study reach. The northern dam is referred to as the Iowa Power dam and the southern dam is referred to as the Burlington Street dam. The City of Iowa City provided plan sets for both dams which included cross-sectional information and spatial orientation. Burlington Street dam plans were referenced to a local datum and had to be adjusted to the 1988 North American Vertical Datum (NAVD). Adjustment of dam elevations were based on GNSS measurement of nearby landmarks. Iowa Power dam plans referenced NAVD 88. Spatial orientation of the dam matched the existing DTM based on georeferenced aerial

photographs and the location of adjacent structures present in the DTM. Dam elevations were added to the existing DTM using breaklines, a series of geospatially-referenced edges to which topographic data must conform, in ArcGIS.

### 3.5.2 Location of bridge piers

Twelve major bridges exist along the Iowa River channel in the study area. Cross-sectional information and locations of abutments and piers were provided by the City of Iowa City, the City of Coralville, Cedar Rapids and Iowa City Railway Company, Iowa Northern Railway Company and the Iowa Department of Transportation. Because abutment data was already included in the Ayres DTM, no modification to the DTM was made in the vicinity of the bridge abutments. Spatial orientation of bridge piers was estimated using cross-sectional information at the up- and down-stream edges of the piers and georeferenced aerial photos. No elevation information was required, because bridge piers were treated as no-flow areas in the numerical model. Therefore, only a georeferenced perimeter of each bridge pier was determined.

### 3.5.3 Creek geometry modification in the vicinity of culverts

Six culverts exist along Ralston Creek within the study area. While the majority of creek geometry was included in the Ayres DTM, creek geometry beneath the culverts was unknown. Creek geometry beneath the culverts was required to prevent flow blockage in Ralston Creek. The author used upstream and downstream creek geometry to manually estimate the geometry directly beneath each culvert. Figure 3.6 displays the modification process.

### 3.5.4 Inclusion of buildings

Thousands of buildings exist within the study area. The City of Iowa City, the City of Coralville, and the University of Iowa provided the author with georeferenced polygons delineating the exterior of all buildings on file. Aerial maps of the study area, provided by the Iowa State University Geographic Map Server (ISU GIS Facility 1999-

2009), were used to locate and digitize newly constructed buildings that were not included in municipal records.

Two DEMs were created using the existing DTM and the building data. The first DEM, primary used in the numerical model, did not include buildings within the study area and was generated directly from the DTM. The second DEM, discussed in Chapter 4, included all buildings as extruded objects. ArcGIS was used to extrude buildings from the original DTM surface to create the second DEM. Because elevation data for buildings was not available, the buildings were extruded a constant distance of 3 m from the DTM surface.

The Saint Venant equations are invalidated when flow occurs over steep floodplain geometry (Lai 2009). Thus, in an effort to maintain the assumptions of the numerical code, the buildings were extruded with sloping, rather than vertical, walls. A constant slope of 2:1 was used for all extruded buildings. First, all polygons representing building footprints were buffered 1.5 m horizontally. Next, the DTM elevation was mapped to the buffer polygons and the original polygons were used to create breaklines. The DTM elevation was also mapped to the original building footprint polygons. The maximum elevation of each individual structure footprint was calculated as a new attribute. Then 3 m was added to this elevation. A new DEM was generated, using the breaklines and polygons with new elevation attributes. Figure 3.7 displays the modification process.

## 3.6 Water surface elevation surveys

Three water surface elevation surveys of the Iowa River were conducted in support of the investigation: an aerial LiDAR survey and two GNSS surveys. Figure 3.8 displays coverage of the 2008 LiDAR survey and both GNSS surveys. The figure also displays river stationing, established to quantify the distance between individual GNSS measurements of the water surface elevation.

The aerial LiDAR survey was conducted by the National Center for Airborne Laser Mapping (NCALM) during the falling peak of the 2008 flood hydrograph. The survey extends 20 km south along the Iowa River from the Coralville Lake. The western edge of the study area, in the vicinity of Clear Creek, was not included. Krajewski, et al. (2009) developed an algorithm to derive accurate flood extend and inundation depth from the LiDAR data. LiDAR data points were classified into flooded and non-flooded categories and water depth was calculated for flooded points. A raster was generated from the flooded points, values representing water depth. Inundation extent was also determined based on the spatial distribution of flooded points.

Immediately after the 2008 flood peak, Ayres Associates performed a GNSS survey of high water marks along the Iowa River within the study area. Vertical and horizontal survey controls were established using the Johnson County, Iowa GNSS control network.

In early September 2009, Coralville Lake discharged to the Iowa River at an approximately steady, bankfull condition for three days. The author performed a survey along the Iowa River using RTK GNSS to establish bankfull WSE for numerical model calibration. Water surface elevation was measured at twenty-seven locations along the Iowa River. Vertical and horizontal survey controls were established using the Johnson County, Iowa GNSS control network.

## 3.7 Bulk flow data

Historical discharge rates were obtained for the inflow and outflow boundaries of the study area. USGS discharge data were obtained from a public USACE website (US Army Corp of Engineers 2009). Figure 3.9 displays the 2008 flood hydrographs for Iowa River and Clear Creek. The figure also displays the times at which the high water mark GNSS survey and the aerial LiDAR survey, discussed in Section 3.6, were conducted. The Iowa River was the only significant outflow in the study area. A rating curve for the Iowa River near the model outflow, generated by FEMA (2007) is presented as Figure

3.10. While historical stage data were available for Rapid Creek, only current and historical maximum discharge data were available. No discharge data were available for Ralston Creek.

## 3.8 Summary

A large-scale data collection and compilation effort has been conducted to support current and future numerical simulations of the Iowa River corridor in the vicinity of Iowa City. A single-beam bathymetric survey of the Iowa River was conducted from the outlet of Coralville Lake to the southern corporate limit of Iowa City. A multi-beam bathymetric survey of the Iowa River in the vicinity of the University of Iowa and downtown Iowa City was also conducted. A bathymetric map with varying resolution was generated for the entire study reach. Topographic information, in the form of high-resolution photogrammetric survey data and contour maps of various resolutions were combined with bathymetric data to generate a DTM. Spillways and bridge piers were manually added to the DTM based on plans obtained from the City of Iowa City, the City of Coralville, Cedar Rapids and Iowa City Railway Company, Iowa Northern Railway Company and the Iowa Department of Transportation. Tributary creek geometry was added beneath culverts and buildings within the study area were extruded from the DTM. Three water surface elevation surveys of the Iowa River at various flow rates were conducted in support of the investigation. Bulk flow data were obtained from USGS-operated stream gages and a preexisting rating curve.

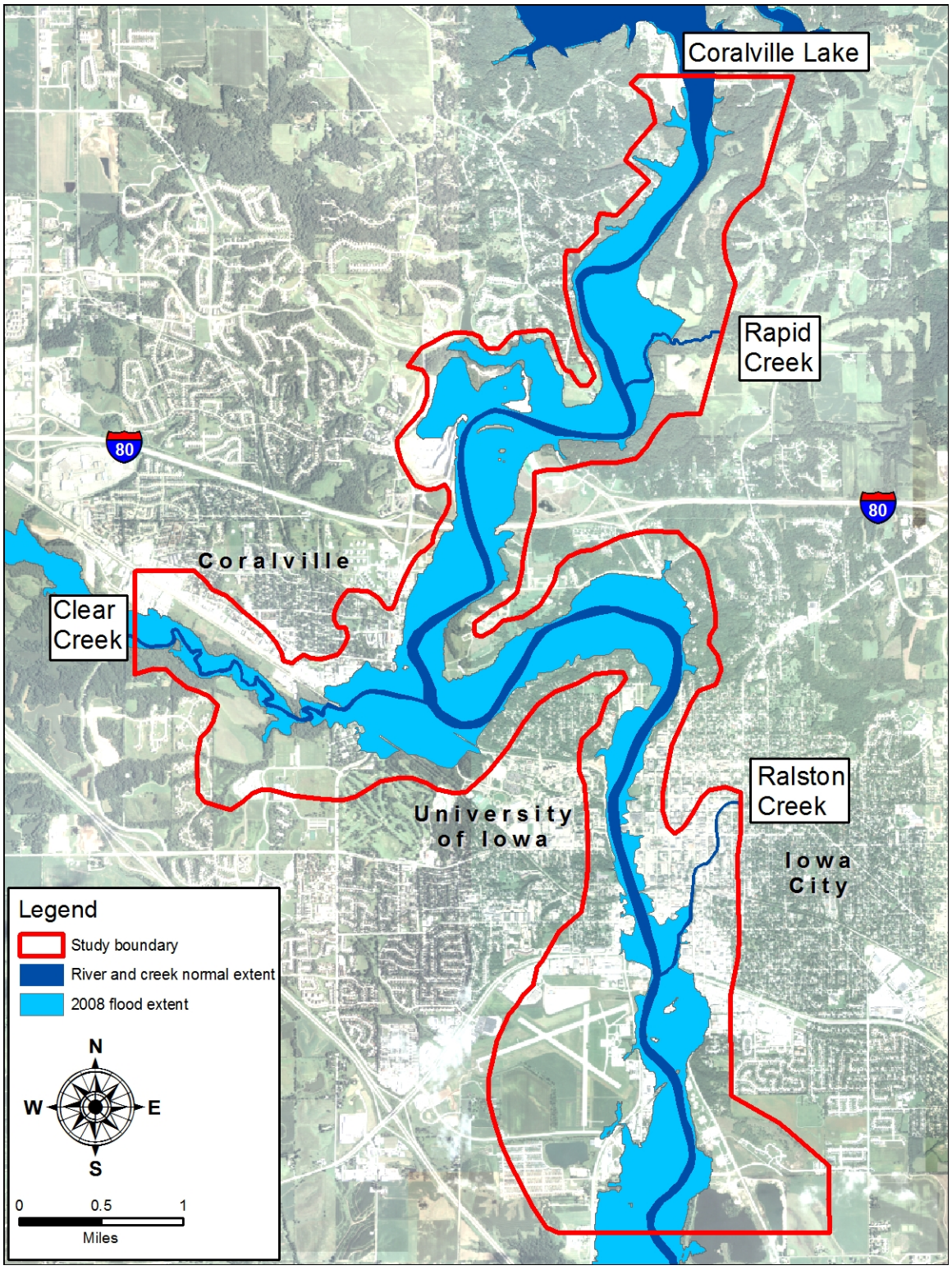


Figure 3.1. Aerial view of the study area.

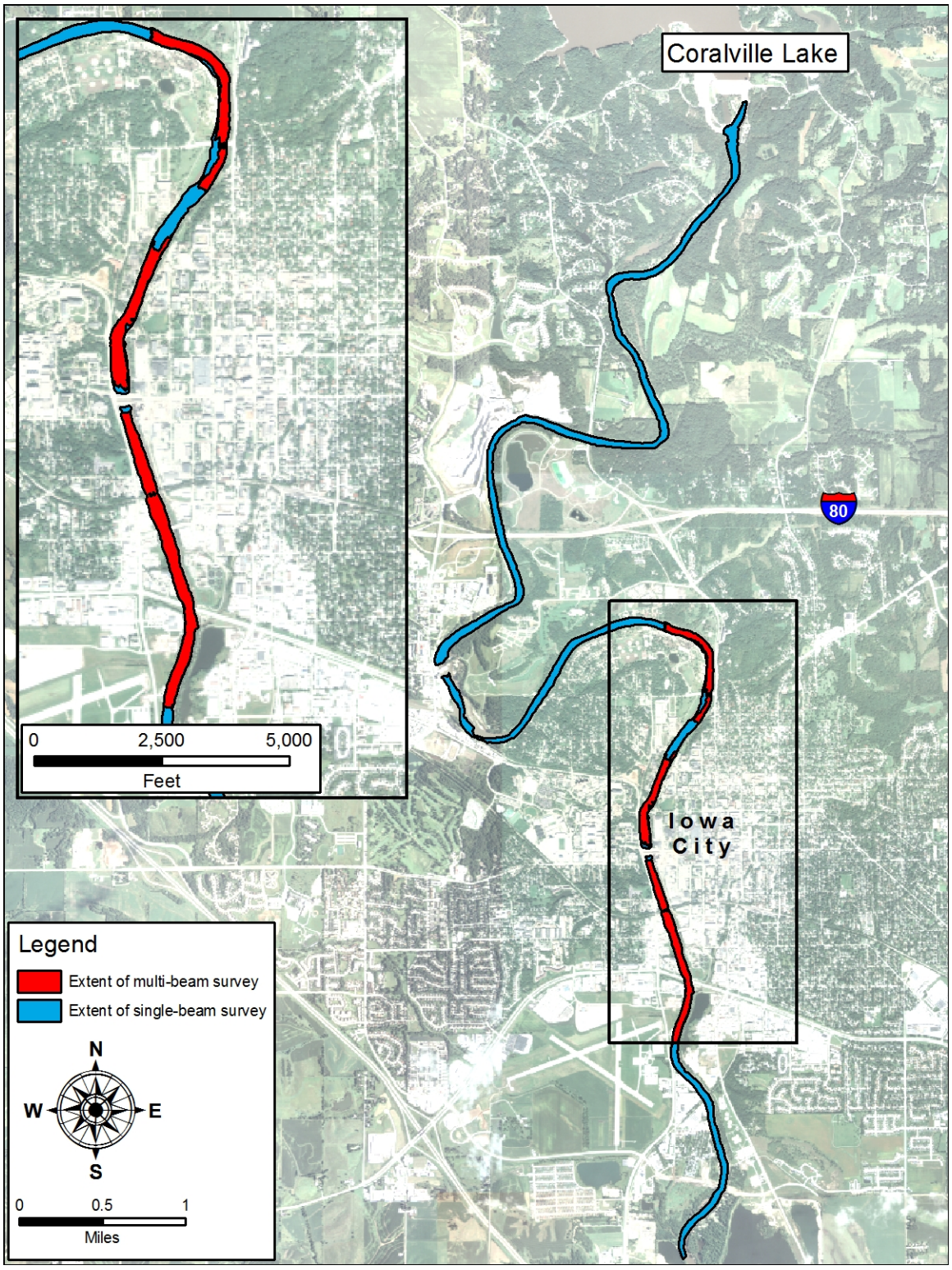


Figure 3.2. Extent of Iowa River single- and multi-beam bathymetric surveys.

Table 3.1. Hydrographic system equipment uncertainties.

| System Component | Measurement Type | Uncertainty* |
|---|---|---|
| Trimble R8 GNSS | Horizontal Position | 10mm |
| | Vertical Position | 20mm |
| RESON SeaBat 7125 multi-beam echosounder | Depth | 6mm |
| Odom HT100 single-beam echosounder | Depth | 10mm ± 0.01% depth |
| Applanix POS MV inertial positioning system | Roll and Pitch | 0.010° |
| | Heave | 50cm |
| | Position | 20-100mm |

*Uncertainty values obtained from manufacturer fact sheets.

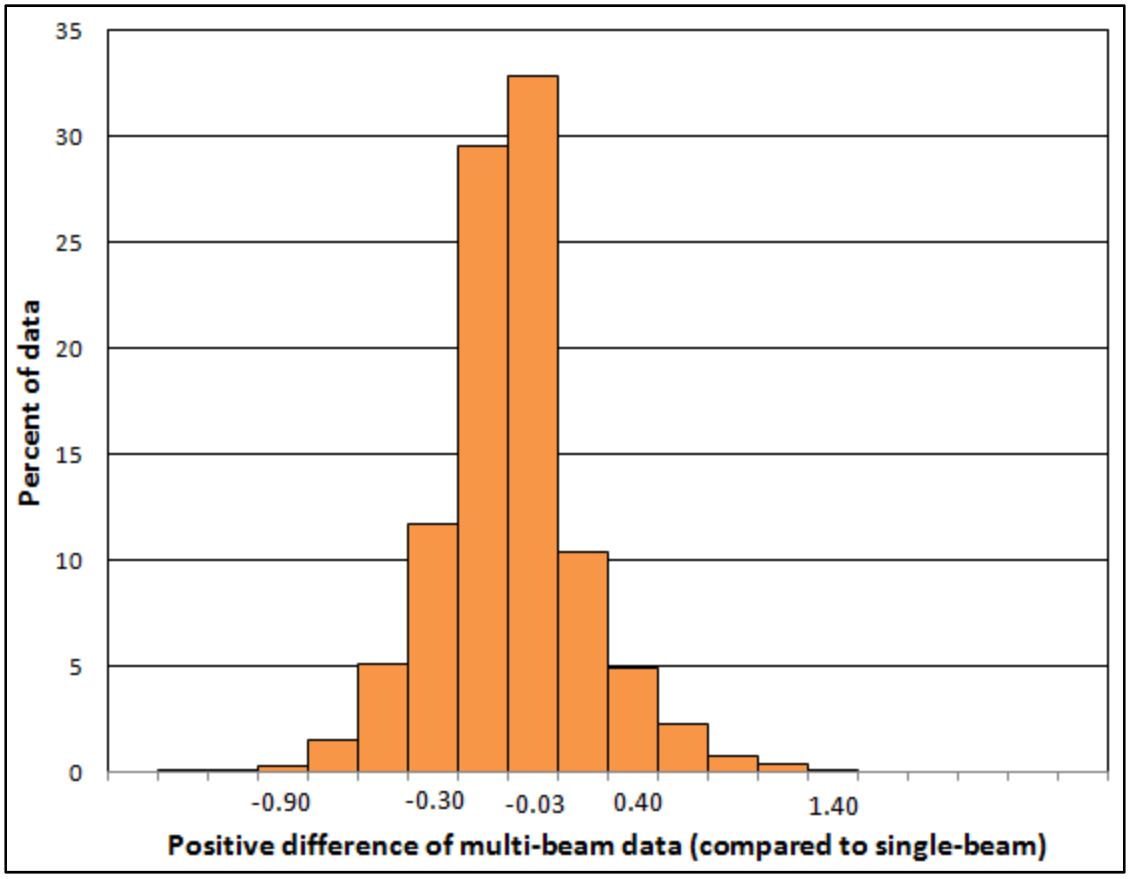


Figure 3.3. Difference between Iowa River bed elevations measured using multi- and single-beam hydrographic survey systems (multi-beam minus single-beam, m).

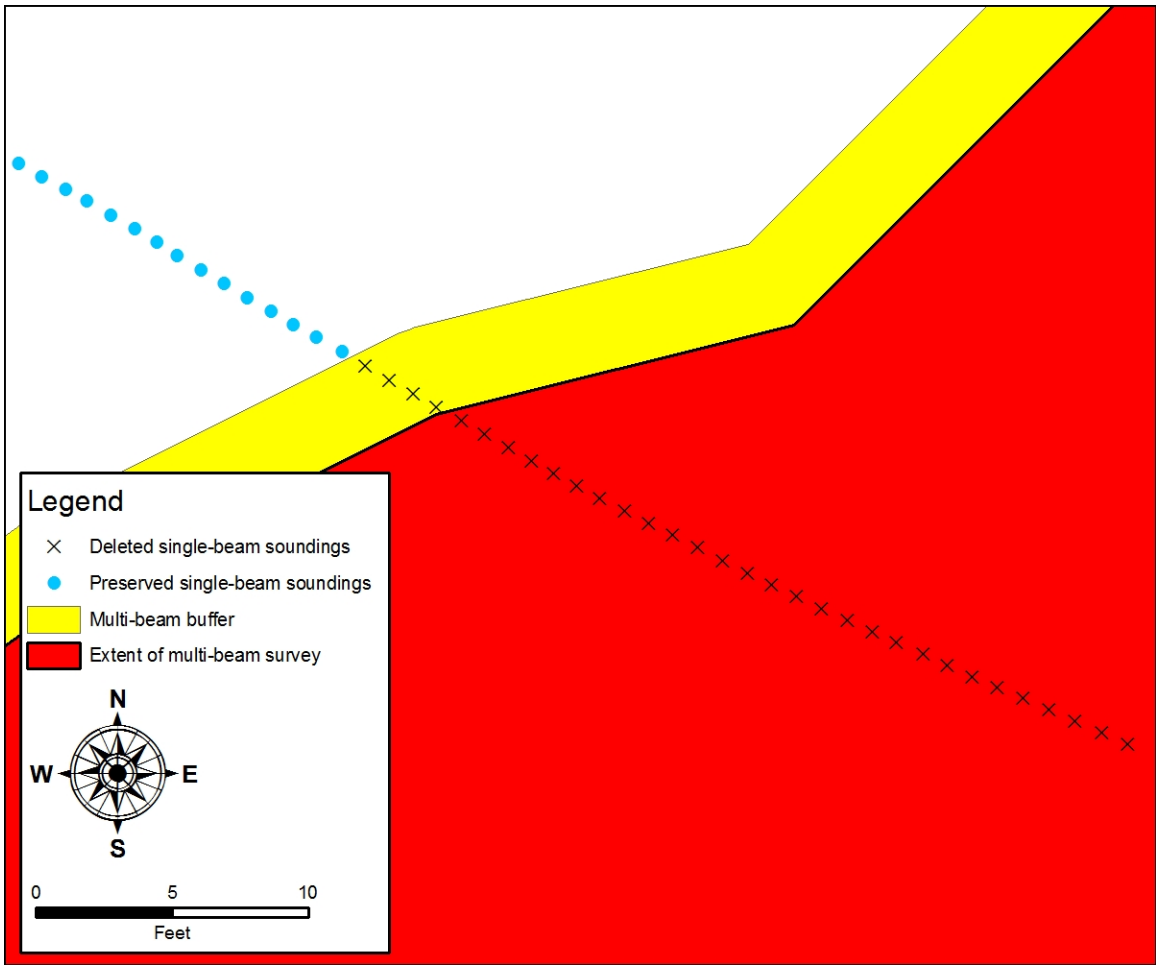


Figure 3.4. Demonstration of treatment used to address overlapping bathymetry from single- and multi-beam surveys prior to DEM construction.

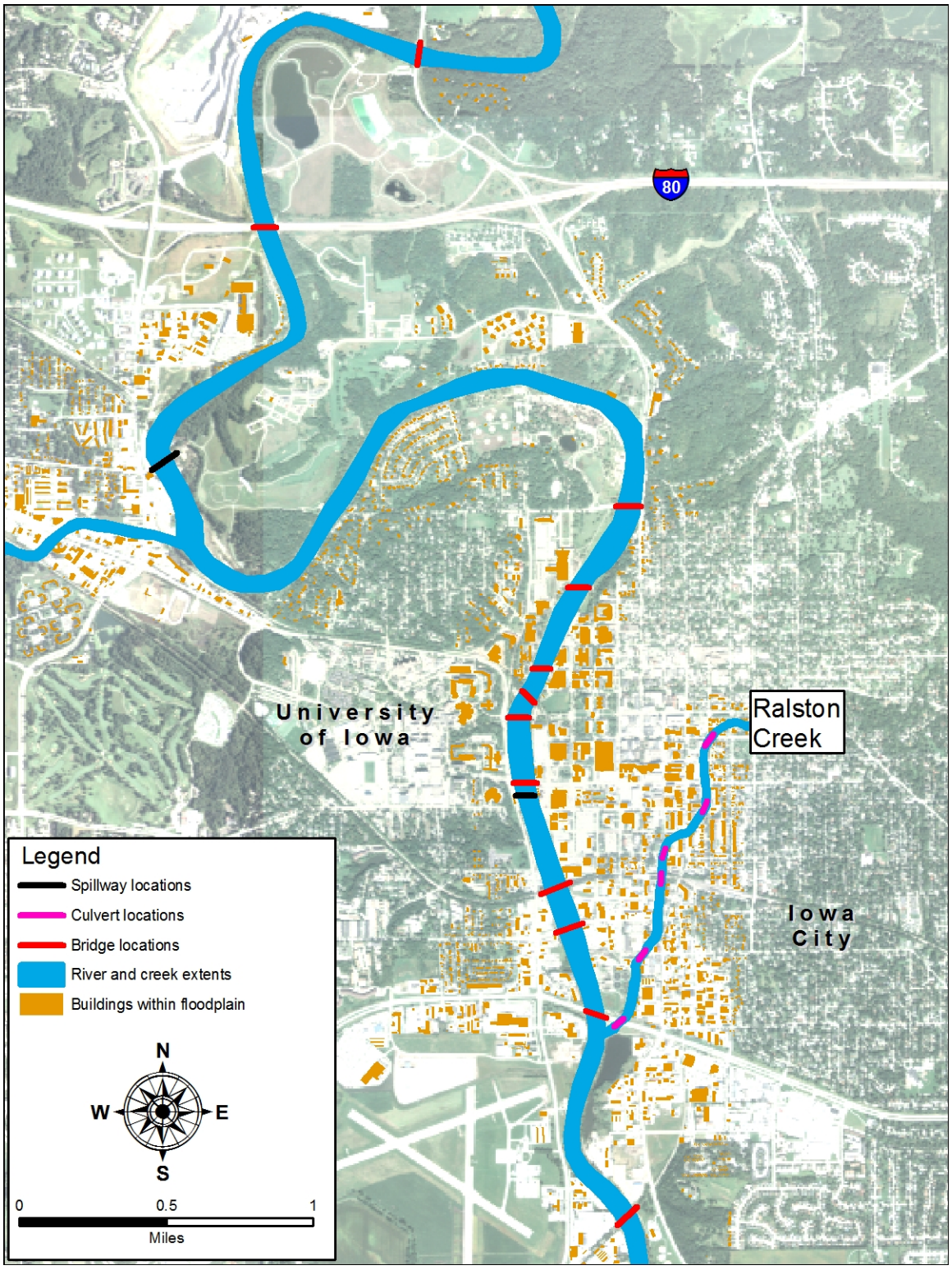


Figure 3.5. Locations of low head dams, bridges, culverts, and buildings in the study reach.

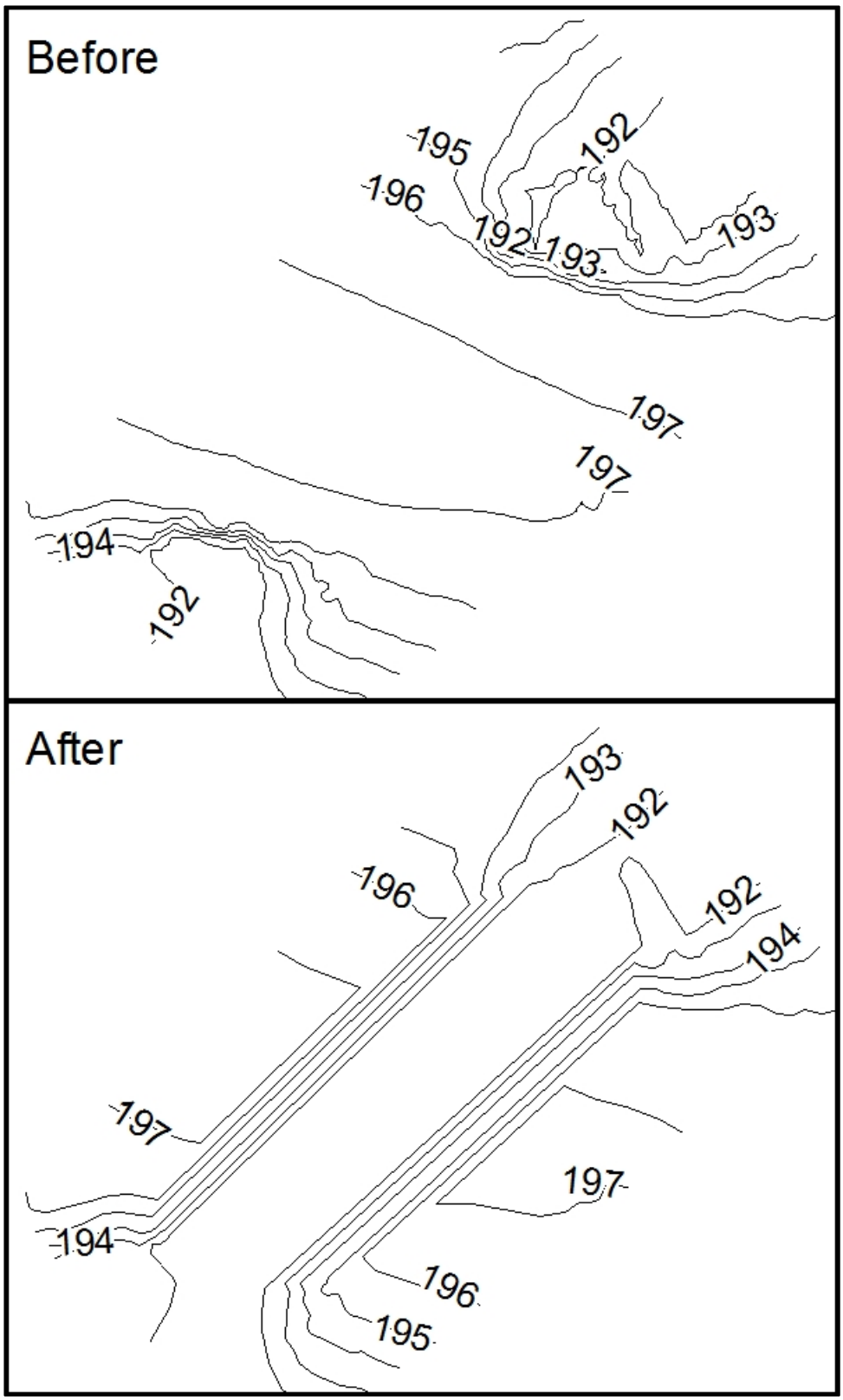


Figure 3.6. Example of DTM modifications made to remove artificial blockages in Ralston Creek caused by culverts.

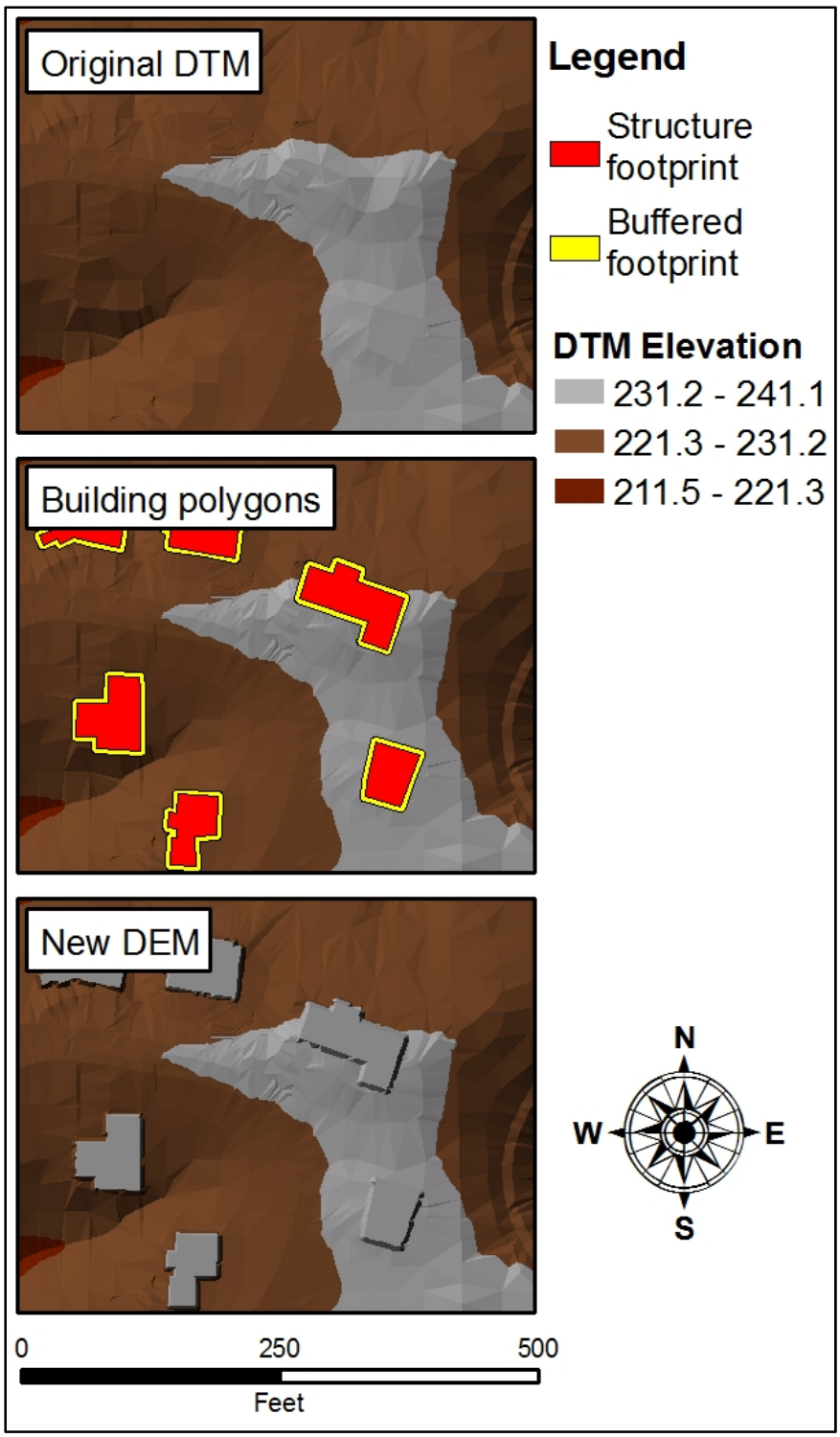


Figure 3.7. Example of DTM modification made to include buildings in the floodplain.

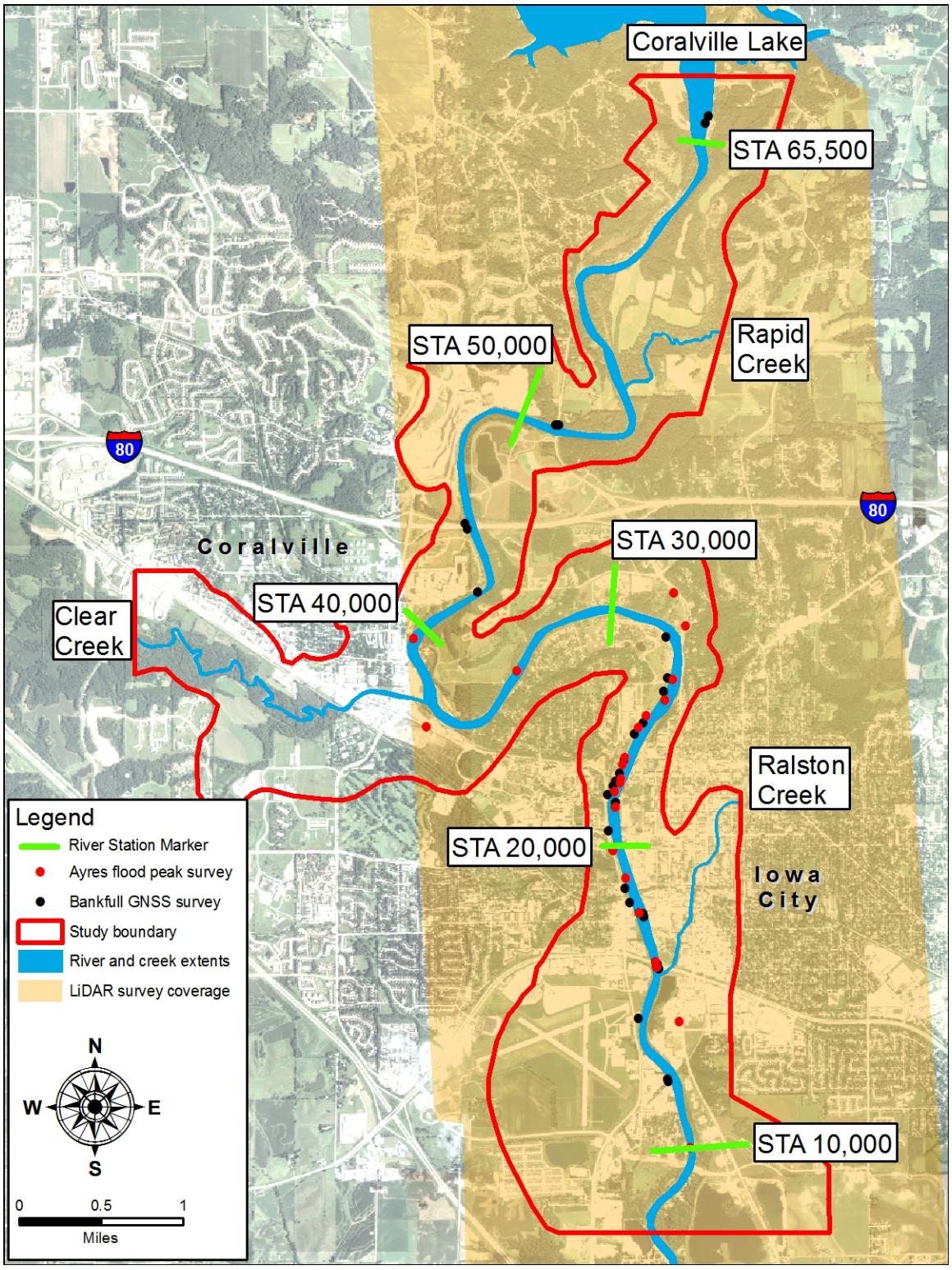


Figure 3.8. Extent of aerial LiDAR survey and RTK GNSS within the study reach.

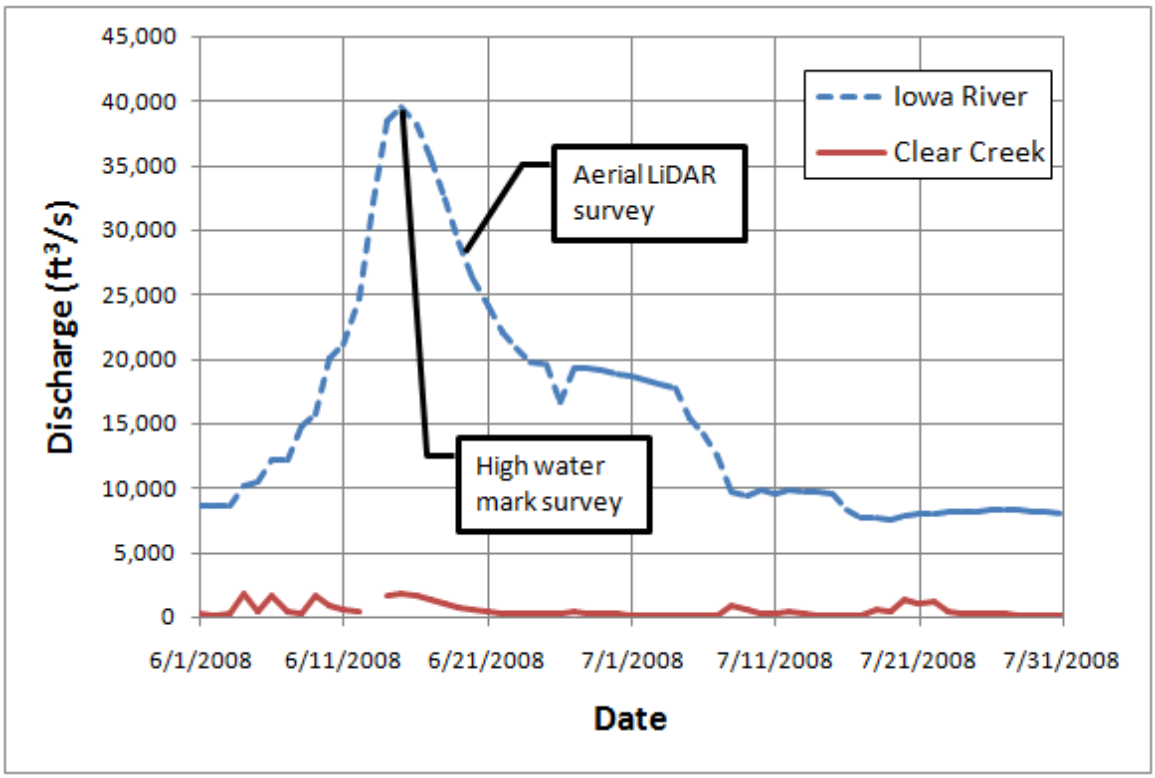


Figure 3.9. Iowa River and Clear Creek 2008 discharge hydrograph.

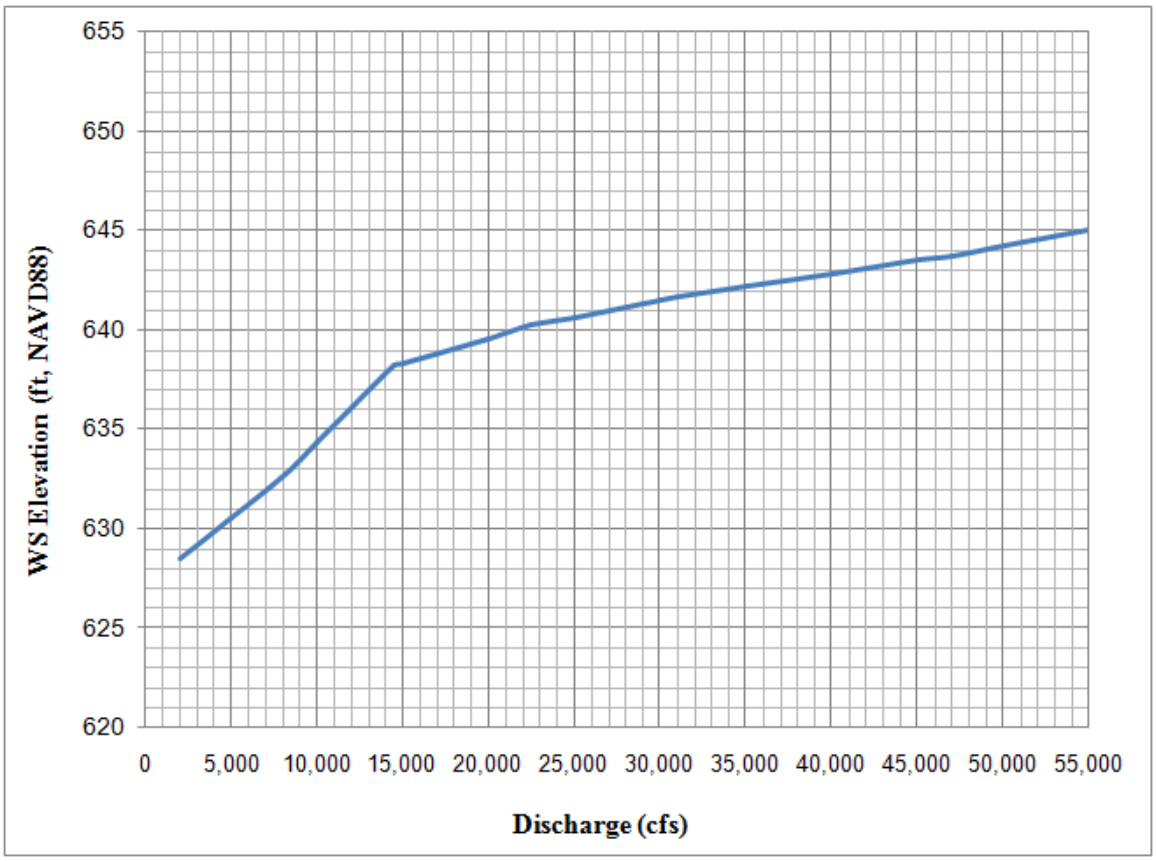


Figure 3.10. Iowa River rating curve from flood insurance study (FEMA 2007) at the downstream model boundary.

# CHAPTER 4: NUMERICAL SIMULATION

The DEM without extruded buildings was used to create a numerical model of hydraulic flow through the study reach. The DEM with extruded buildings was used in a later comparison as described in Chapter 4. The numerical model was calibrated using aerial LiDAR and bankfull WSE data and validated using high water marks collected immediately after the peak of the 2008 flood. In the present study, the calibrated model is used to predict the extent and depth of inundation for various flow conditions.

## 4.1 Numerical methods

The model domain includes the area denoted by the study limit presented in Chapter 3. Flow conditions were simulated using the unsteady depth averaged St. Venant equations with a parabolic turbulence model in the SRH-2D software. All computational meshes were generated using SMS 10.0 mesh generation software. Each simulation used an unstructured, hybrid mesh with approximately 550-thousand elements. Use of a hybrid mesh of quadrilateral and triangular cells allowed for greater detail in areas of interest and decreased computation time.

SMS generates computational mesh elements from user-created feature arcs. Feature arcs define internal boundaries (river channel bank, building flootprints) and are manually digitized or converted from ArcGIS shapefiles. The node density of a given feature arc is input by the user. Connected feature arcs that form a closed loop are converted to polygons retaining all nodes defined for the initial feature arcs. Material type (which in turn determines surface roughness) and mesh type (quadrilateral or triangular) are assigned to each polygon. SMS iteratively generates mesh elements within each polygon.

High-resolution aerial photographs were used to delineate material types. Seven material types were used: river, field, woods, pavement, light development, medium development, and heavy development. Figure 4.1 displays the spatial distribution of material types in the numerical model. Feature arcs were placed along borders between

different materials. Node density was selected to satisfy computational constraints and to capture critical geometric features (e.g. narrow alleys). Low node density (~20 m) was used in rural areas with few or no buildings and high node density (~5 m) was used in urbanized areas. A node density of ~8 m was selected for the Iowa River channel, except in the vicinity of narrow bridge piers and the two spillways, where node density was increased to ~5 m to more accurately represent pier and spillway geometry. Node density along Iowa River banks was increased to ~4 m to increase performance at bankfull flow conditions. A node density of 4 m to 6 m was used in all tributary channels included in the numerical model.

Modifications to the numerical mesh were required to represent buildings as no-flow areas. Most building footprints included protrusions or features that would not be captured by the minimum overbank mesh resolution of 5 m. Additionally, buildings in residential areas were often spaced closer than 5 m apart. Thus buildings less than 5 m apart were considered to be one continuous structure. All building polygons within the 2008 flood limit were buffered 2.5 m in ArcGIS and dissolved to connect any overlapping polygons. Polygon resolution was reduced using ArcGIS advanced editor. The buffered, dissolved, and generalized polygons were then inversely buffered 2.5 m to retain their original size. Thus feature arcs that approximately define building footprints while maintaining a minimum mesh resolution of 5 m were generated. Figure 4.2 displays the polygon generalization process. The final building polygons were imported into SMS and classified as no-flow areas in the numerical mesh.

## 4.2 Boundary conditions

Discharges from Coralville Lake, Clear Creek, Ralston Creek, and Rapid Creek were simulated as inflows to the numerical model. Table 4.1 lists the steady-state discharges used in the investigation. Historical USGS gage data were used as simulated inflows from Coralville Lake and Clear Creek. Maximum historical discharges were used as the inflows for Rapid Creek for all extreme event simulations, and a discharge value

recorded at the time of the bankfull RTK survey was used for the bankfull simulation. Because no discharge data were available for Ralston Creek, inflow was assumed to be equal to Rapid Creek, as the two creeks have similar drainage areas. A single outflow boundary condition was simulated at the southern edge of the numerical model. The outflow boundary condition was represented by the FEMA-established rating curve. All other boundary conditions not specified as an inflow or outflow were represented as a no-slip wall conditions. Because the limits of the numerical model extended beyond those of the 2008 flood no-slip walls did not affect simulation results.

## 4.3 Simulation run-time

Simulation run-time required to reach a steady-state condition was determined for (1) a bankfull condition and (2) the flood peak. Both discharge scenarios were simulated as steady inflows for 100 hours using a desktop computer with two 2.67 GHz Quad-Core Intel Xeon processors and 12 GB of memory. A WSE monitor point was placed near the outlet of the model. When the WSE did not visibly change, it was assumed that the model had reached an approximate steady-state. To confirm this assumption, WSE for the previous hour was subtracted from most recent WSE output file at every mesh node. The comparisons resulted in a mean difference 0.000004 m and a standard deviation of 0.00006 m for the bankfull condition and a mean difference of 0.001 m and a standard deviation of 0.015 m for the flood peak. Using the aforementioned computer, a run-time of 62 hours for extreme event simulations and 48 hours for bankfull flow was sufficient to reach a steady-state condition.

## 4.4 Model calibration

SRH-2D requires selection of Manning's 'n' values to model bed friction losses. Initial Manning's 'n' values for the river channels and natural floodplains were selected from a list of established values (Chow 1959). Roughness coefficients for urban floodplains were estimated based on a previous investigation of urban flooding with channelized flow in streets and alleys (Calenda, Mancini and Volpi 2005). Table 4.2 lists

the initial ‘n’ values. The numerical model was calibrated for (1) a bankfull flow condition and (2) an extreme flood event. The initial ‘n’ values were iteratively modified and corresponding simulation results were compared to WSE data. Final ‘n’ values were selected based on the simulation that best matched the WSE data. Calibration procedures are described in detail in Chapter 4.

### 4.4.1 Bankfull calibration

The 2009 bankfull WSE survey data were used to calibrate the numerical model to a bankfull flow condition. After an initial series of bankfull simulations with varying ‘n’ values were performed, none of the simulation results upstream of the Burlington Street and Iowa Power spillways agreed with the WSE survey data. The author theorized that the spillway elevations were incorrect. The crest of the Burlington Street spillway, including flashboards that were not included in the original plan set, was measured with GNSS and found to be 0.6 m higher than originally estimated. The Burlington Street spillway crest was adjusted to the measured value and model calibration resumed. Six values of ‘n’ for the river channel were selected and the river discharges measured at the time of the GNSS survey were simulated.

Table 4.3 lists the 'n' values used in each bankfull simulation and computed difference between simulated and measured WSE at each survey location. Stationing refers to river stationing defined in Figure 3.8. A Manning's 'n' value of 0.030 resulted in the lowest sum difference between simulated and measured WSE and was selected as the river channel 'n' value.

### 4.4.2 Iowa Power spillway elevation adjustment

The elevation of the Iowa Power spillway crest was iteratively modified, using the selected river channel 'n' value of 0.030, until the simulation results agreed with the WSE survey. The Iowa Power spillway crest was thus increased by 0.34 m. Because the Iowa Power spillway crest was modified based on a channel 'n' value of 0.030, the upper portion of the numerical model cannot be considered calibrated. However, it is unlikely that the roughness of the river bed changes significantly over the study reach, because the 'n' value of 0.030 still resulted in the lowest sum of difference between simulated and measured WSE for the reach below the Iowa Power spillway. Thus the channel 'n' value of 0.030 was used for the entire study reach.

### 4.4.3 Extreme flood event calibration

The aerial LiDAR survey data was used to calibrate the numerical model to an extreme flood event. Because six 'n' values were used in the overbank area of the numerical model, modifying values individually was not feasible. Therefore all initial overbank values of 'n' were multiplied by a common factor and the river discharges measured at the time of the LiDAR survey were simulated. Deviation from the LiDAR-derived WSE data was calculated for each mesh node.

Table 4.4 lists the multiplication factor and the 'n' values used in each overbank simulation, as well as the mean over-prediction of the simulation and the standard deviation. The original 'n' values, used in simulation "iv", resulted in the lowest mean value of -0.01 m.

## 4.5 Model validation

The calibrated numerical model was validated using the WSE survey performed by Ayres Associates immediately following the 2008 flood peak. The 2008 peak discharges from Coralville Lake, Clear Creek, Rapid Creek and Ralston Creek were simulated as steady model inflows. A comparison of the simulated and measured 2008 peak WSE data is presented in Figure 4.3. The comparison resulted in a mean simulated under-prediction of 0.01 m, a standard deviation of 0.10 m and a maximum difference of 0.14 m. Based on the validation results, the numerical model reasonably predicts the flood WSE in the study reach.

## 4.6 Model application

The present study was initiated to develop a high-resolution numerical model that can accurately and precisely predict depth and velocity during flood events in the Iowa City area. Maps of depth and velocity can be generated to facilitate long-term flood mitigation and the model can be used to predict depth and velocity on a daily basis during a flood event to facilitate near real-time mitigation and emergency management. As an example, Figure 4.4 displays inundation depth at the peak of the 2008 flood and Figure 4.5 displays velocity magnitude. As the insets in both figures display, local depth and velocity can be predicted, which will allow emergency managers to better assess potential safety hazards and property damage. The model will be used to generate a library of static inundation maps to better communicate flood forecast information, and as a tool to design and evaluate flood mitigation alternatives. The model is also under evaluation for integration with basin-scale hydrologic models as part of a flood forecasting system.

## 4.7 Turbulent eddy viscosity coefficient sensitivity analysis

The parabolic turbulence model used in SRH-2D requires the selection of α, a turbulent eddy viscosity coefficient. The default value for α is 0.7, which was used for all final simulations based on the findings of Lai (2009): most numerical simulations are not sensitive to $\alpha$ and using the default value is recommended. Values of α in SRH-2D can range from 0.3 to 1.0. A sensitivity analysis of α was conducted by performing three simulations of the same steady-state discharge scenario. The first simulation used the default value of α. The second and third simulations used the minimum and maximum values of α, respectively. Inundation depth was exported from SRH-2D for each node and "dry" nodes were assigned a depth value of 0 m. Nodes where both inundation values were 0 m were removed from the comparison.

Figure 4.6 displays a graphical comparison of the sensitivity analysis simulations. The difference between water depths for most nodes was negligible, but there was an appreciable difference in water depth for some nodes with shallow (less than 3 m) depths. The most common difference in water depth was 0.2 m. Figures 4.7 and 4.8 display difference in simulated water depth (compared to depth using the default value) using the minimum and maximum value of α, respectively. The green circles denote areas where a difference of depth of 0.2 m or greater occurred. In both comparisons, significant differences in depth occurred in the vicinity of the University of Iowa arts campus and an industrial area near the southern Iowa City corporate limit. In the comparison of simulated depth using the minimum value of α, significant difference also occurred in a portion of the Coralville business district.

Figure 4.9 displays velocity magnitude (using the default value of α) as a function of difference in depth between simulations using the default value and the minimum and maximum values, respectively. Red color indicates data in the areas of interest as denoted in Figures 4.7 and 4.8. As the Saint-Venant equations in Chapter 2 describe, eddy viscosity is used to calculate turbulent stress terms. Mathematical relationships between

turbulent stress terms and velocity suggest lower velocity magnitudes in these areas may contribute to increased sensitivity to eddy viscosity. While the data in Figure 4.9 indicate a relationship between low velocity and difference in inundation depth, further investigation of the sensitivity to turbulent eddy viscosity should be performed.

## 4.8 Investigations

The calibrated, validated numerical model was used in multiple investigations. First, the effect of Rapid and Ralston Creeks was investigated to determine if the lack of historic discharge data significantly affected simulation results. Second, the treatment of buildings in the floodplain was investigated to determine if a less physically consistent representation of buildings can be used without significantly decreasing simulation accuracy. Third, 2D simulation results from the 2008 flood, the previous flood of record and the 100 year and 500 year discharges (as defined by FEMA) were compared to results from an existing 1D model developed by Ayres Associates to assess the benefit of using a 2D model. Finally, a steady-state simulation of the discharge during the LiDAR survey was compared to two unsteady 2008 flood simulations to justify the assumption that a steady-state simulation can accurately represent an unsteady flow condition.

### 4.8.1 Effect of Rapid and Ralston Creeks

During the calibration and validation process, the author assumed that the discharges from Rapid and Ralston Creeks did not significantly affect simulation results. The validity of this assumption was tested by comparing a simulation where the historical maximum discharge for both creeks was included to a simulation where no discharge for either creek was included. A histogram displaying the increase in depth due to the inclusion of Rapid and Ralston Creeks is presented as Figure 4.10. Appreciable differences in depth (greater than 0.1 m) occurred in approximately 6 percent of all mesh cells, but no significant difference in depth occurred in the remaining portion of cells. It was therefore concluded that lack of historic discharge data for minor creeks did not affect simulation accuracy.

### 4.8.2 Effect of buildings

Buildings were represented as no-flow areas in the computational mesh, as described in Chapter 3, to maximize fidelity of the numerical model. However, the process of delineating and removing buildings is time consuming. Thus the effect of removing buildings from the numerical model is assessed to balance efficiency and model fidelity in future flood inundation investigations. A new computational mesh was generated from the DEM that included buildings as extrusions from the land surface. Building outlines were delineated in the mesh but computational elements within the building boundaries were not removed from flow computations. A comparison of simulation results is presented as Figure 4.11. Appreciable differences in depth (greater than 0.1 m) occurred at lesser inundation depths and differences in depth decreased as depth increased. Reach scale simulation results are not affected by the removal of buildings from flow computations, but local inconsistencies occur in shallow water if buildings are not removed from computations. Figure 4.12 displays local differences in water depth around the perimeter of buildings. Significant differences are artifacts of the sloped edge of the buildings discussed in Chapter 3 and are indicative of the method used to generate the DEM, not simulation inaccuracy. As the figure displays, some buildings experienced inundation greater than the extruded height of 3 m and were overtopped in the simulation.

### 4.8.3 Comparison to one-dimensional simulation results

Simulation results were compared to results from an existing 1D model of the study reach. Both the 1D and 2D models were compared to the 2008 peak discharge to determine which model can more accurately predict extreme flood events. Differences from individual high water mark measurements were calculated for both models. The 1D and 2D models resulted in a mean over-prediction of 0.02 m and 0.01 m, respectively, and a standard deviation of 0.31 m and 0.10 m, respectively. The 2D simulation predicted inundation WSE with greater accuracy and precision. This is notable, as the 1D model

was calibrated using the 2008 high water marks. This indicates that high-resolution WSE data, such as LiDAR, can significantly improve numerical model calibration.

Both models were used to simulate peak discharge from an extreme event in 1993 and extreme events with reoccurrence intervals of 100 and 500 years, as defined by FEMA. Because the 2D simulation predicted the 2008 flood peak WSE with greater accuracy and precision, 1D results were compared to the 2D results for the additional discharge scenarios. Table 4.5 lists the mean over-prediction and standard deviation of the 1D simulation results as compared to the 2D simulation. High standard deviations (up to 0.71 m) indicate the 1D model's inability to accurately predict inundation depth throughout the entire study area.

### 4.8.4 Comparison of steady and unsteady flow rates

When the author calibrated and validated the numerical model, steady-state simulations were used and results were compared to measured water surface elevations from unsteady discharges. This process inherently assumed that a steady-state simulation can approximate an unsteady hydraulic condition. The author compared the results from the steady-state simulation to two unsteady simulations. The hydrographs for the two unsteady simulations are presented in Figure 4.13. The first unsteady simulation used the hydrograph from a bankfull condition to the time of the LiDAR survey and is referred to as "full hydrograph". The second unsteady simulated used the hydrograph from the peak of the 2008 flood to the time of the LiDAR survey and is referred to as "partial hydrograph". A fit measure, defined in Equation 4.1, has been used to quantify the ability of the numerical simulations to accurately predict inundation extent (Bates and Roo 2000; Gallegos, Schubert and Sanders 2009).

$$Fit = \frac{A_{measured} \bigcap A_{simulated}}{A_{measured} \bigcup A_{simulated}} \tag{4.1}$$

In the equation above, *Fit* is the fit measure (percent), $A_{measured}$ is the measured inundation area, $A_{simulated}$ is the simulated inundation area, $\cap$ is the intersection of the two areas and $\cup$ is the union of the two areas. The fit measure was used to assess the ability of the simulations to represent the inundation area extracted from the LiDAR data. The full hydrograph fit the LiDAR data 7.9 percent better than the steady simulation and the partial hydrograph fit the data 5.8 percent better than the steady simulation. The increase in fit between the partial hydrograph and the steady-state simulation is greater than the increase between the full hydrograph and the partial hydrograph. While the full hydrograph provides the best result, the large computation time (27 days) is not feasible for most investigations.

### 4.8.5 Effect of hysteresis in the floodplain

Hysteresis, or path dependence, is common in flood events. Due to differences in downstream backwater effects, a specific flow rate on the rising limb of a flood hydrograph will not cause the same inundation extent and depth as the same flow rate on the falling limb of the hydrograph. Figure 4.14 displays City Park, located just north of the University of Iowa campus, at various flow rates on the rising and falling limbs of the 2008 flood hydrograph. Differences in inundation extent and depth can be clearly seen. Figure 4.15 displays difference plots of the inundation extent and depth for the flow rates in Figure 4.14. Disconnected pools of water would drain into the water table as flood limits receded. However, the numerical model cannot account for this drainage. Therefore, in both figures, disconnected areas of inundation were removed from the falling limb of the hydrograph. The two figures explicitly show that steady-state flood simulations, while good estimates of unsteady flow conditions, cannot completely describe inundation extents and depths that will be experienced. If future floods are to be successfully mitigated, unsteady simulations should be performed with up-to-date hydrodynamic information.

## 4.9 Summary

Flow conditions were simulated using the unsteady depth averaged St. Venant equations with a parabolic turbulence model. Discharges from Coralville Lake, Clear Creek, Ralston Creek, and Rapid Creek were simulated as inflows to the numerical model. High-resolution aerial photographs were used to delineate material types and Manning's 'n' values for the river channels and natural floodplain coverage were selected from a list of established values. Run-time required to approximate a steady-state condition was determined for extreme and bankfull discharges. The 2009 bankfull WSE and aerial LiDAR data were used to calibrate the numerical model to a bankfull and overbank flow condition, respectively. The calibrated numerical model was validated using the WSE survey performed by Ayres Associates immediately following the 2008 flood peak and was used to simulate various discharge scenarios. The calibrated, validated numerical can be used in future long-term flood mitigation planning and to support near real-time emergency management decisions. A sensitivity analysis of turbulent eddy viscosity was also performed.

The numerical model was used in multiple investigations. First, the effect of Rapid and Ralston Creeks was investigated to determine if the lack of historic discharge data significantly affected simulation results. Second, the treatment of buildings in the floodplain was investigated to determine if a less physically consistent representation of buildings can be used without significantly decreasing simulation accuracy. Third, 2D simulation results from the 2008 flood, the previous flood of record and the 100 year and 500 year discharges (as defined by FEMA) were compared to results from an existing 1D model developed by Ayres Associates to assess the benefit of using a 2D model. Finally, a steady-state simulation of the discharge during the LiDAR survey was compared to two unsteady 2008 flood simulations to justify the assumption that a steady-state simulation can accurately represent an unsteady flow condition. Differences in inundation extent and depth for discharges on the rising and falling limbs of the flood hydrograph indicate that

if future floods are to be successfully mitigated, unsteady simulations should be performed with up-to-date hydrodynamic information.

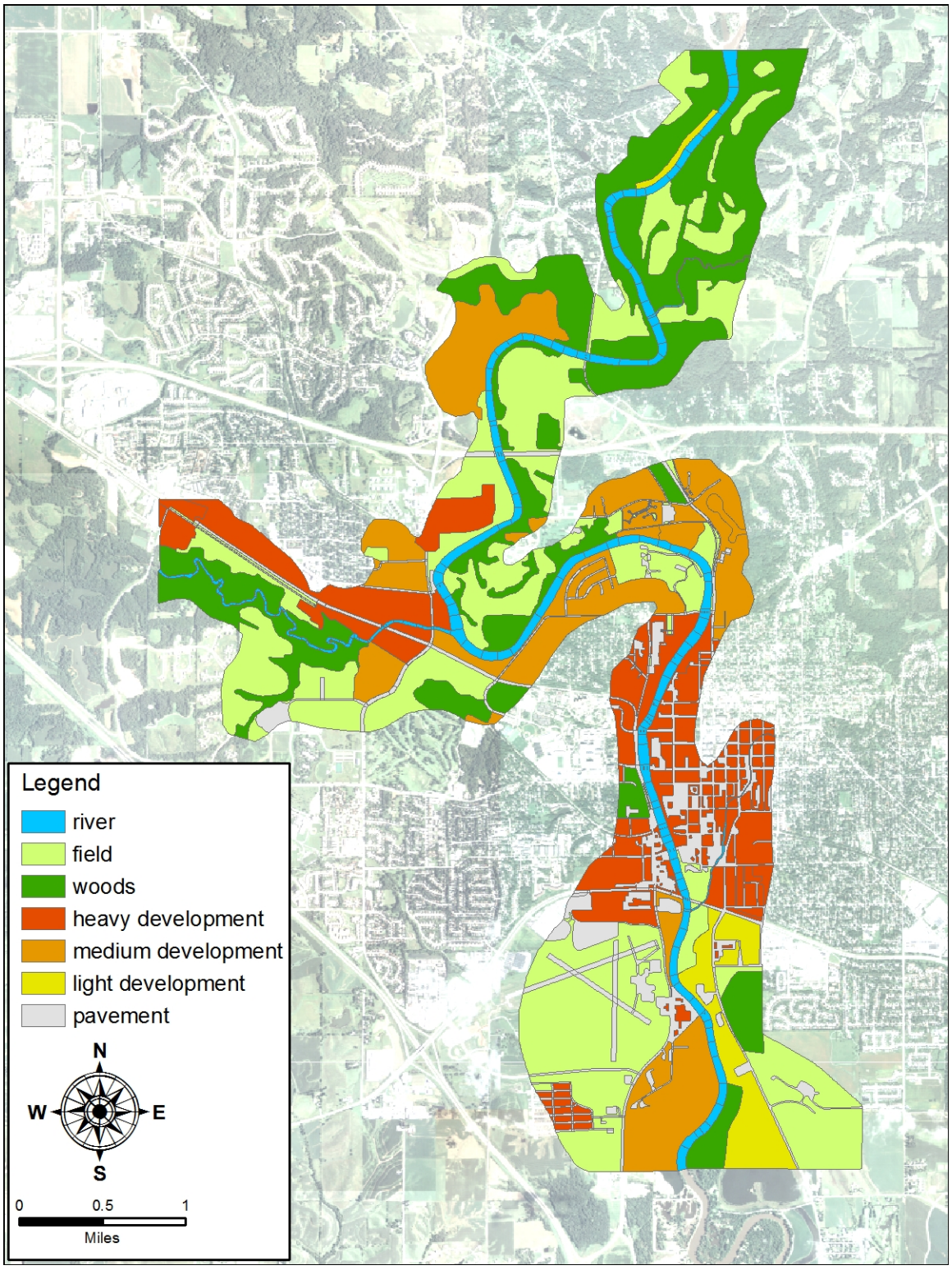


Figure 4.1. Spatial distribution of material types within the study limits.

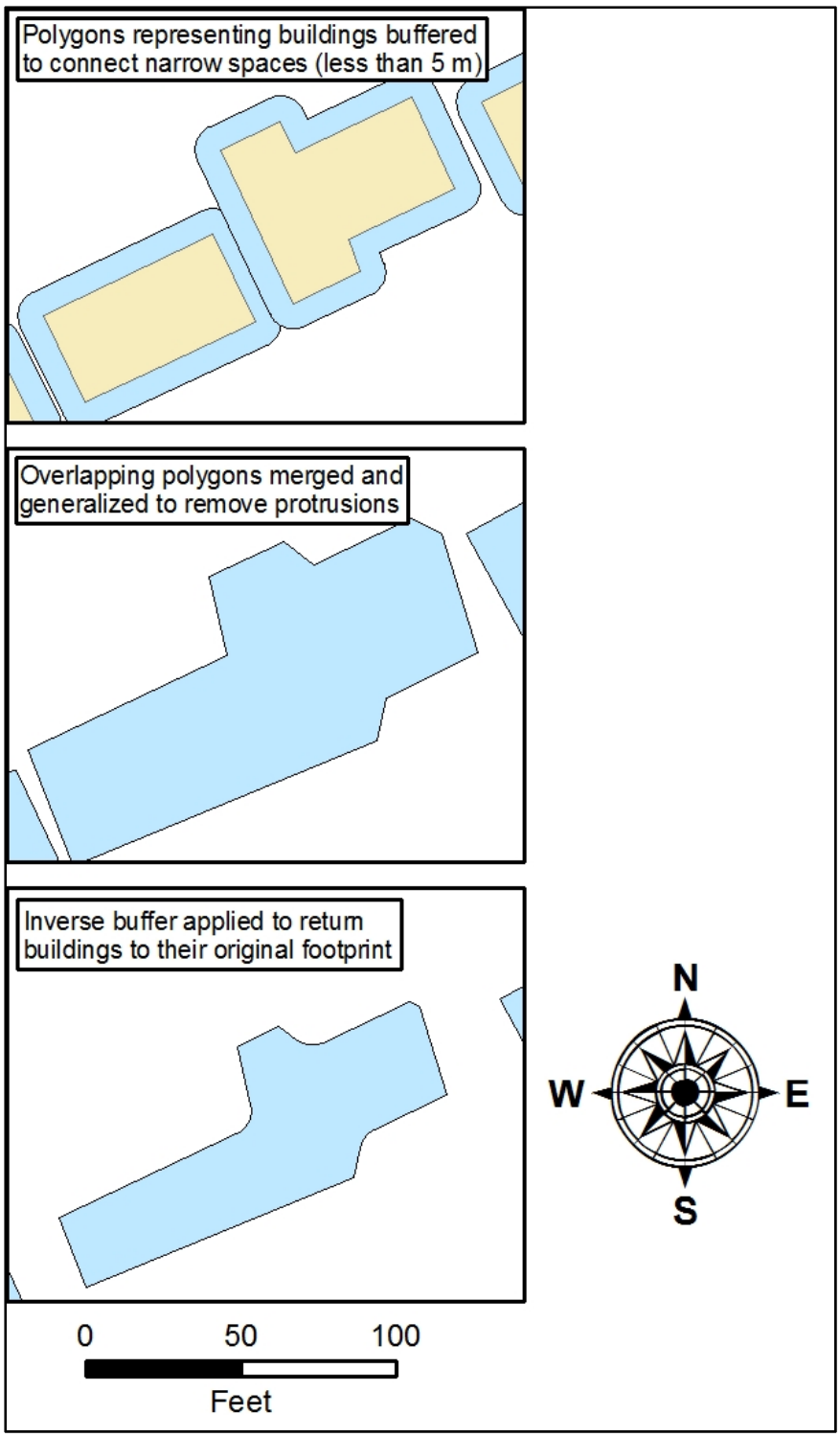


Figure 4.2. Simplification of building footprint.

Table 4.1. Summary of model inlet flow rates.

| Location | Discharge ($ft^3/s$) | | | | | |
|---|---|---|---|---|---|---|
| | Bankfull calib-ration case | LiDAR calib-ration case | 2008 Flood peak validation case | Turbulent eddy viscosity sensitiv-ity case | Effect of creeks case | Effect of buildings case |
| Downstream of Coralville Lake | 5911 | 28128 | 39462 | 29040 | 29040 | 29040 |
| Clear Creek | 108.4 | 646 | 1770 | 717 | 717 | 717 |
| Rapid Creek | 31.8 | 250 | 250 | 250 | 0 | 250 |
| Ralston Creek | 31.8 | 250 | 250 | 250 | 0 | 250 |

Table 4.2. Initial Manning's 'n' values.

| Material Type | Manning's 'n' | Source |
|---|---|---|
| River Channel | 0.035 | Chow 1959 |
| Field | 0.040 | Chow 1959 |
| Woods | 0.120 | Chow 1959 |
| Pavement | 0.013 | Chow 1959 |
| Low Density Development | 0.050 | Calenda, et al. 2005 |
| Medium Density Development | 0.075 | Calenda, et al. 2005 |
| High Density Development | 0.100 | Calenda, et al. 2005 |

Table 4.3. Manning's 'n' calibration values for a bankfull condition.

| | Manning's n value | | | | | |
|---|---|---|---|---|---|---|
| | 0.020 | 0.025 | 0.030 | 0.035 | 0.040 | 0.045 |
| Station | Overestimation of numerical simulation (m) | | | | | |
| 12345 | -0.01 | 0.04 | 0.09 | 0.16 | 0.23 | 0.29 |
| 12562 | -0.06 | -0.01 | 0.05 | 0.11 | 0.18 | 0.25 |
| 14543 | -0.11 | -0.04 | 0.03 | 0.11 | 0.20 | 0.29 |
| 16378 | -0.14 | -0.06 | 0.03 | 0.12 | 0.23 | 0.33 |
| 16637 | -0.14 | -0.06 | 0.03 | 0.13 | 0.23 | 0.34 |
| 18107 | -0.17 | -0.07 | 0.04 | 0.15 | 0.27 | 0.39 |
| 18255 | -0.29 | -0.19 | -0.08 | 0.04 | 0.16 | 0.27 |
| 18677 | -0.15 | -0.05 | 0.07 | 0.18 | 0.30 | 0.42 |
| 19195 | -0.21 | -0.11 | 0.01 | 0.12 | 0.25 | 0.36 |
| 20490 | -0.20 | -0.08 | 0.05 | 0.18 | 0.31 | 0.44 |
| 21093 | -0.12 | -0.11 | -0.10 | -0.09 | -0.08 | -0.07 |
| 22007 | -0.09 | -0.08 | -0.07 | -0.05 | -0.04 | -0.02 |
| 22242 | -0.09 | -0.07 | -0.06 | -0.05 | -0.03 | -0.01 |
| 22490 | -0.07 | -0.06 | -0.04 | -0.03 | -0.01 | 0.01 |
| 22723 | -0.10 | -0.09 | -0.08 | -0.06 | -0.04 | -0.02 |
| 23002 | -0.09 | -0.07 | -0.06 | -0.04 | -0.02 | 0.00 |
| 23453 | -0.05 | -0.03 | -0.01 | 0.01 | 0.03 | 0.06 |
| 24367 | -0.04 | -0.02 | 0.00 | 0.03 | 0.06 | 0.10 |
| 24812 | -0.07 | -0.04 | -0.01 | 0.02 | 0.06 | 0.10 |
| 26083 | -0.10 | -0.06 | -0.01 | 0.04 | 0.09 | 0.14 |
| 26559 | -0.12 | -0.07 | -0.02 | 0.04 | 0.09 | 0.16 |
| 28025 | -0.14 | -0.08 | -0.01 | 0.07 | 0.14 | 0.22 |
| 42692 | -0.03 | -0.02 | -0.01 | 0.01 | 0.02 | 0.04 |
| 44977 | 0.01 | 0.03 | 0.04 | 0.07 | 0.09 | 0.12 |
| 45320 | -0.03 | -0.01 | 0.01 | 0.04 | 0.06 | 0.09 |
| 51715 | -0.09 | -0.05 | -0.01 | 0.04 | 0.09 | 0.15 |
| 51470 | -0.08 | -0.04 | 0.00 | 0.05 | 0.10 | 0.16 |
| | Sum of deviation from measured WSE (m) | | | | | |
| | 2.75 | 1.62 | 1.02 | 2.01 | 3.42 | 4.85 |
| | Sum of deviation from measured WSE (m) | | | | | |
| | 0.07 | 0.04 | 0.05 | 0.08 | 0.11 | 0.15 |

Table 4.4. Manning's 'n' calibration values for an extreme event.

| Simulation designation | Multi-plication factor | Manning's 'n' | | | | | | | Simulation overprediction (m) | |
|---|---|---|---|---|---|---|---|---|---|---|
| | | River Channel | Field | Woods | Pave-ment | Low Density Develop-ment | Medium Density Develop-ment | High Density Develop-ment | mean | standard devation |
| i | 0.7 | 0.035 | 0.028 | 0.084 | 0.009 | 0.035 | 0.053 | 0.070 | -0.49 | 0.36 |
| ii | 0.8 | 0.035 | 0.032 | 0.096 | 0.010 | 0.040 | 0.060 | 0.080 | -0.34 | 0.33 |
| iii | 0.9 | 0.035 | 0.036 | 0.108 | 0.012 | 0.045 | 0.068 | 0.090 | -0.17 | 0.30 |
| iv | 1.0 | 0.035 | 0.040 | 0.120 | 0.013 | 0.050 | 0.075 | 0.100 | -0.01 | 0.29 |
| v | 1.1 | 0.035 | 0.044 | 0.132 | 0.014 | 0.055 | 0.083 | 0.110 | 0.16 | 0.29 |
| vi | 1.2 | 0.035 | 0.048 | 0.144 | 0.016 | 0.060 | 0.090 | 0.120 | 0.32 | 0.27 |
| vii | 1.3 | 0.035 | 0.052 | 0.156 | 0.017 | 0.065 | 0.098 | 0.130 | 0.44 | 0.30 |

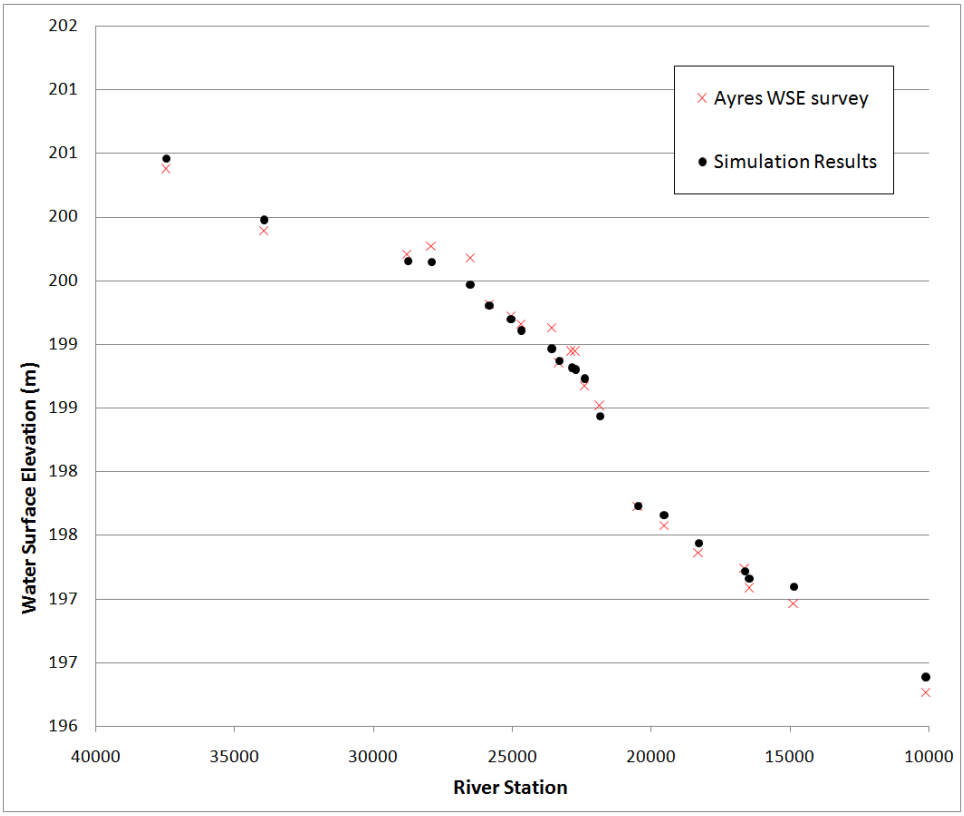


Figure 4.3. Comparison of measured and calibrated 2008 peak WSE data.

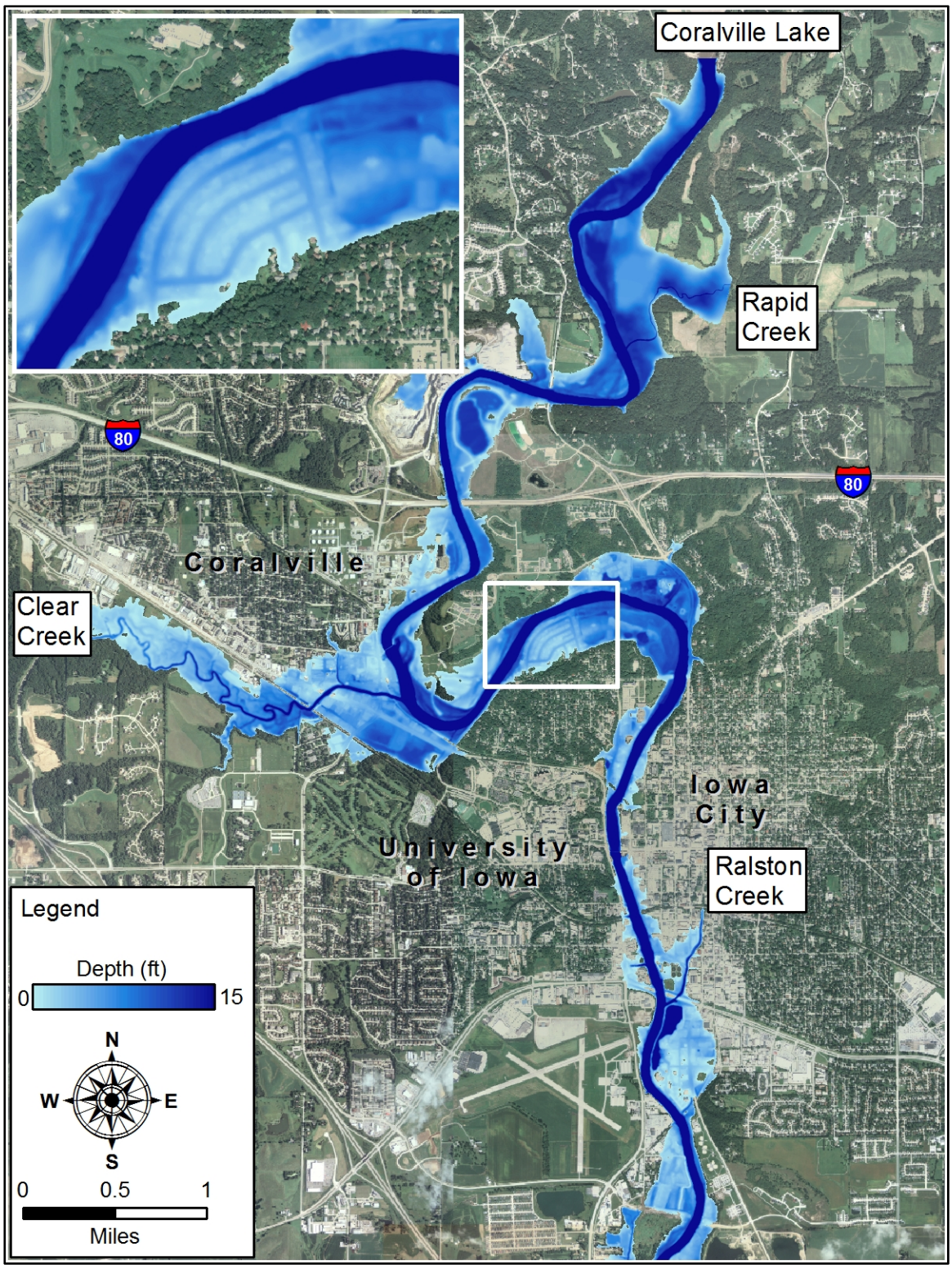


Figure 4.4. Inundation depth during the 2008 flood peak.

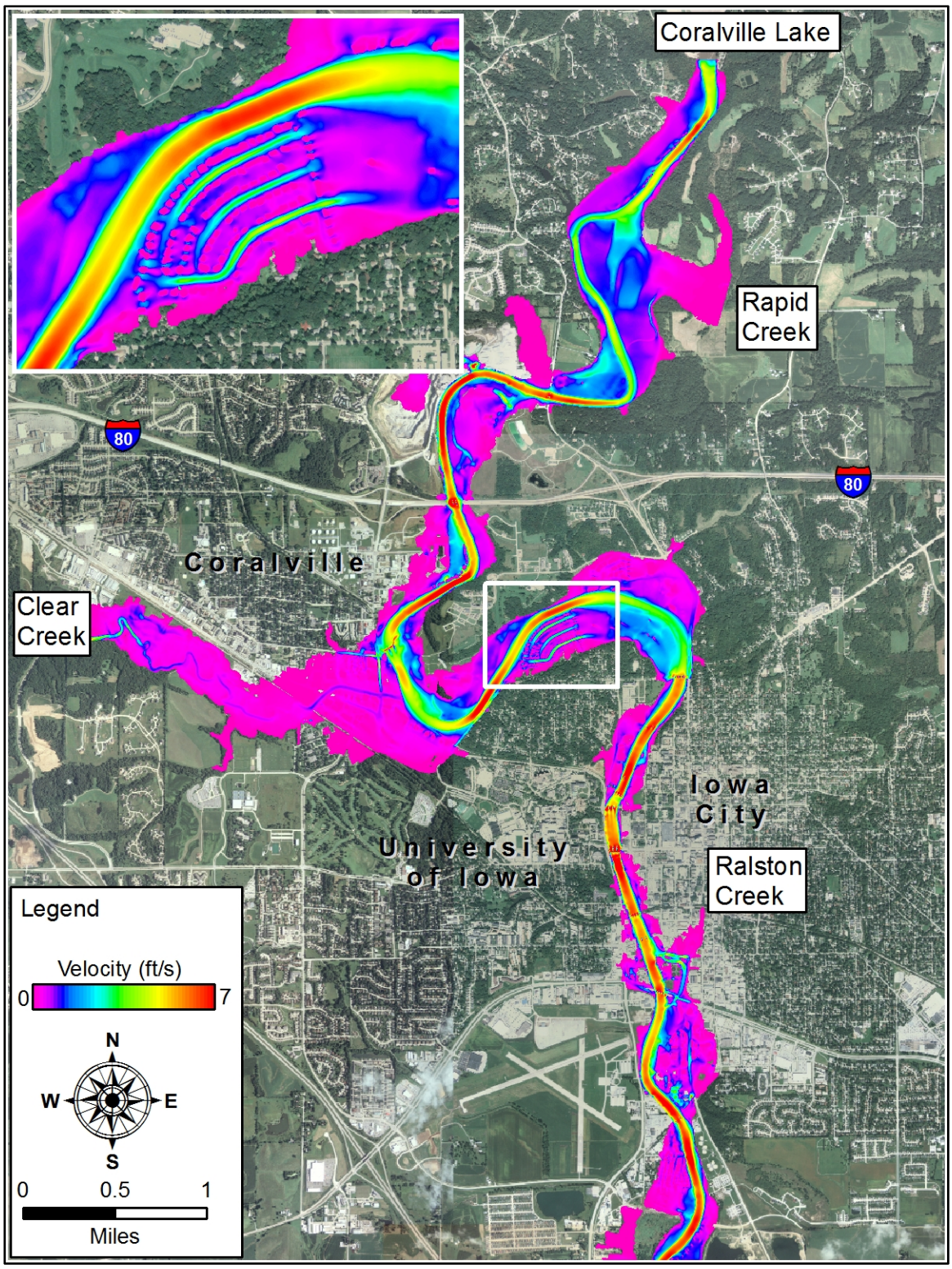


Figure 4.5. Velocity during the 2008 flood peak.

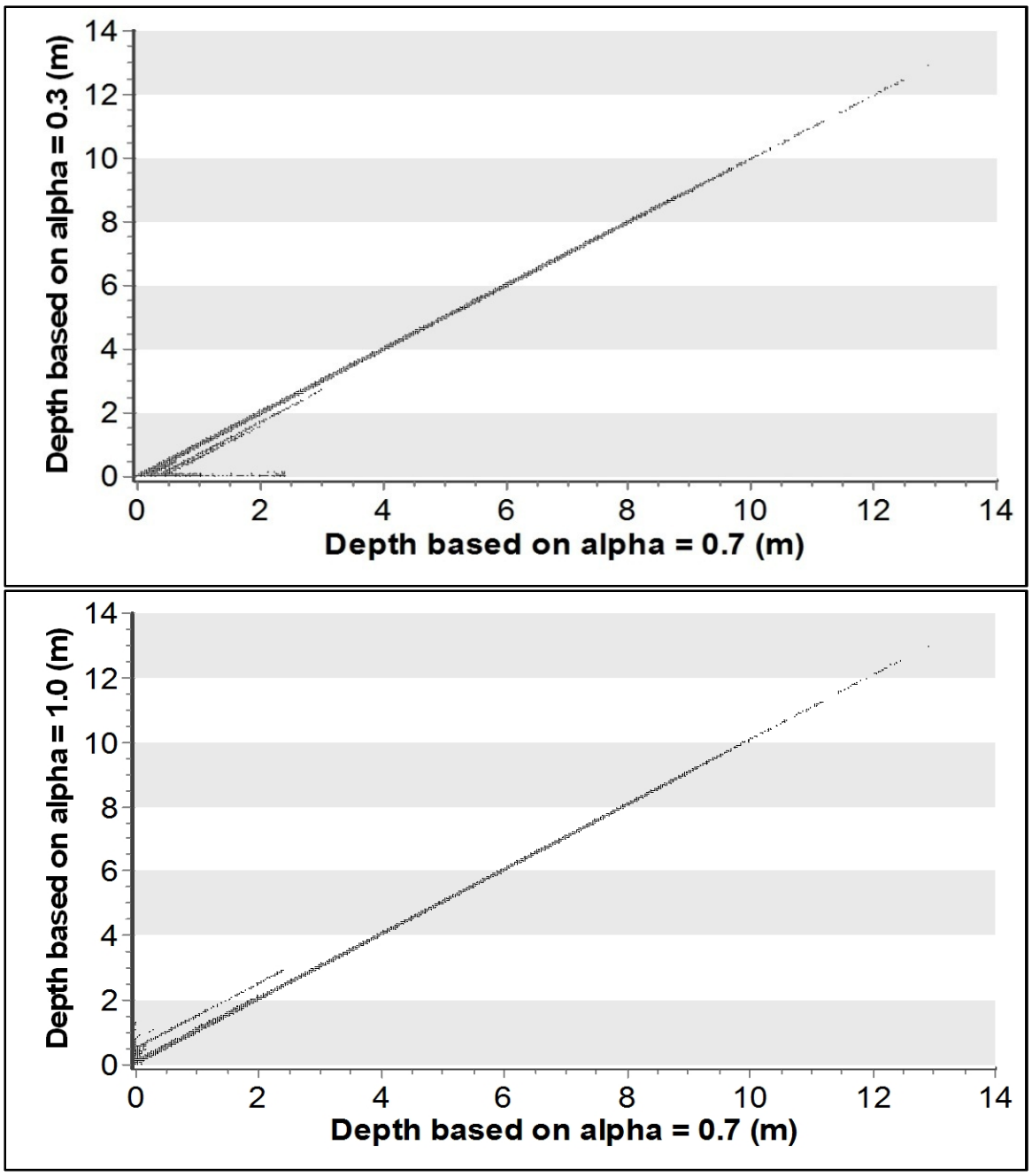


Figure 4.6. Comparison of results from the turbulent eddy viscosity coefficient sensitivity analysis.

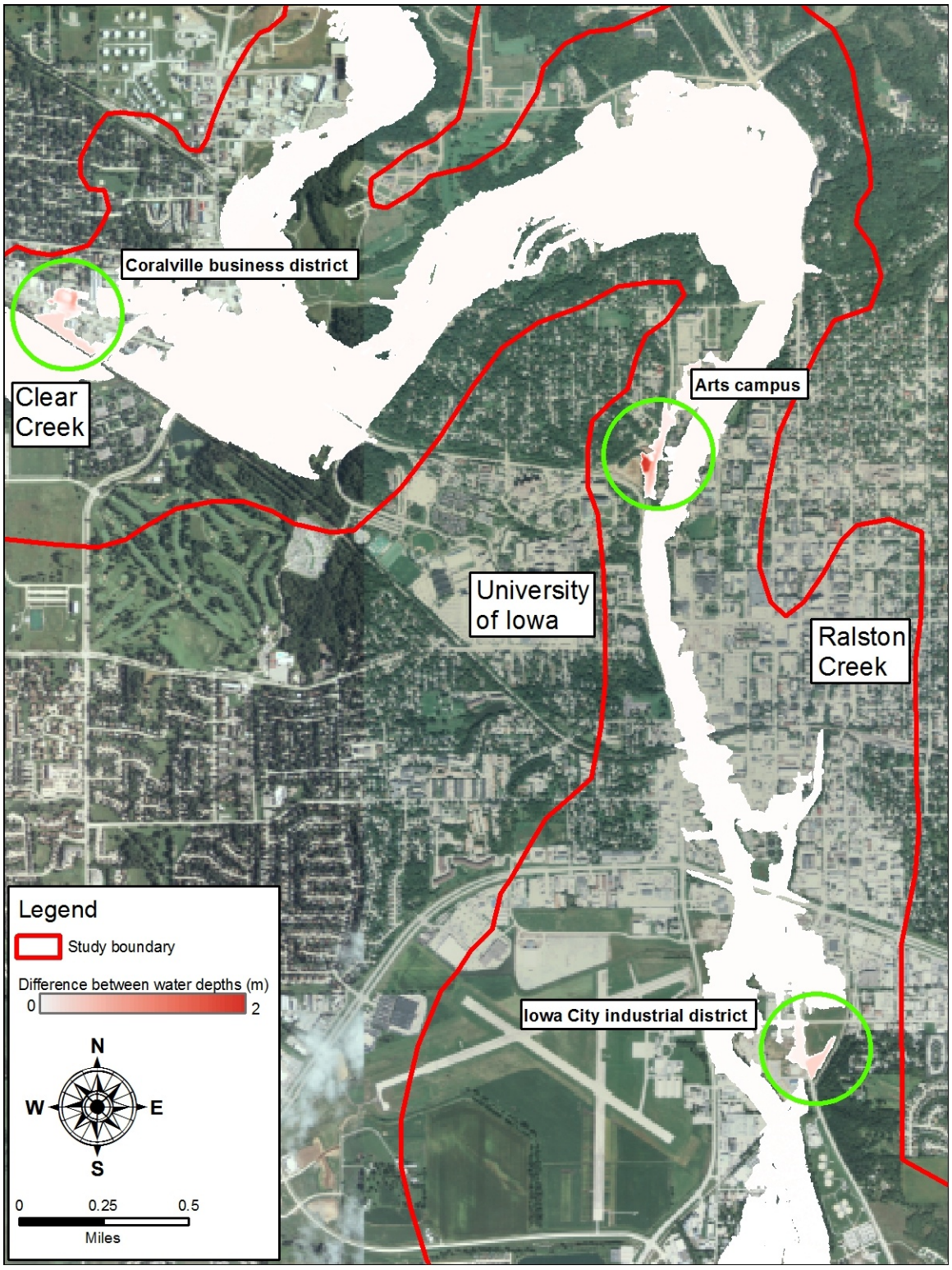


Figure 4.7. Simulated water depth using a turbulent eddy viscosity coefficient of 0.3 subtracted from water depth using a coefficient of 0.7 (difference in m).

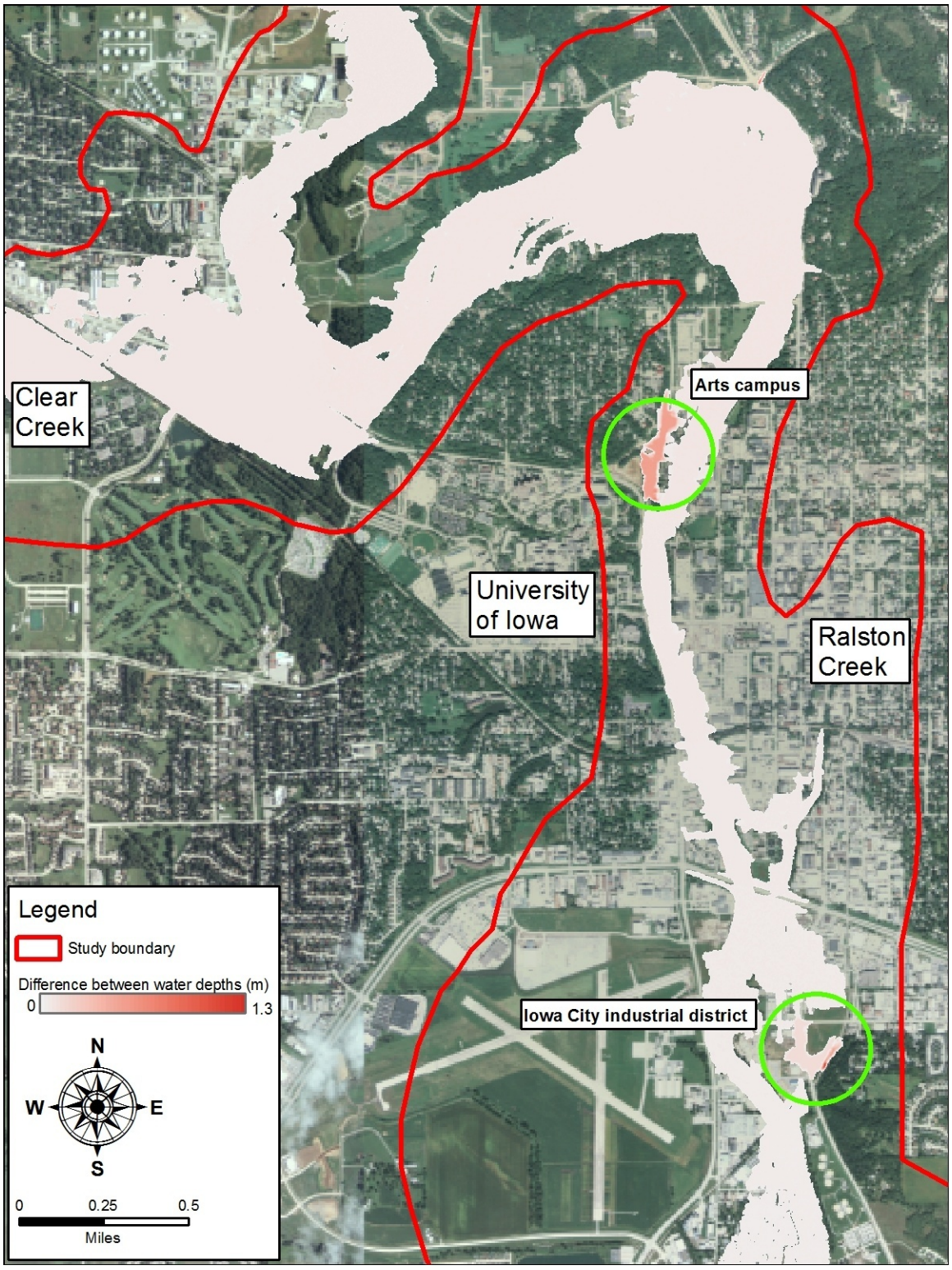


Figure 4.8. Simulated water depth using a turbulent eddy viscosity coefficient of 0.7 subtracted from water depth using a coefficient of 1.0 (difference in m).

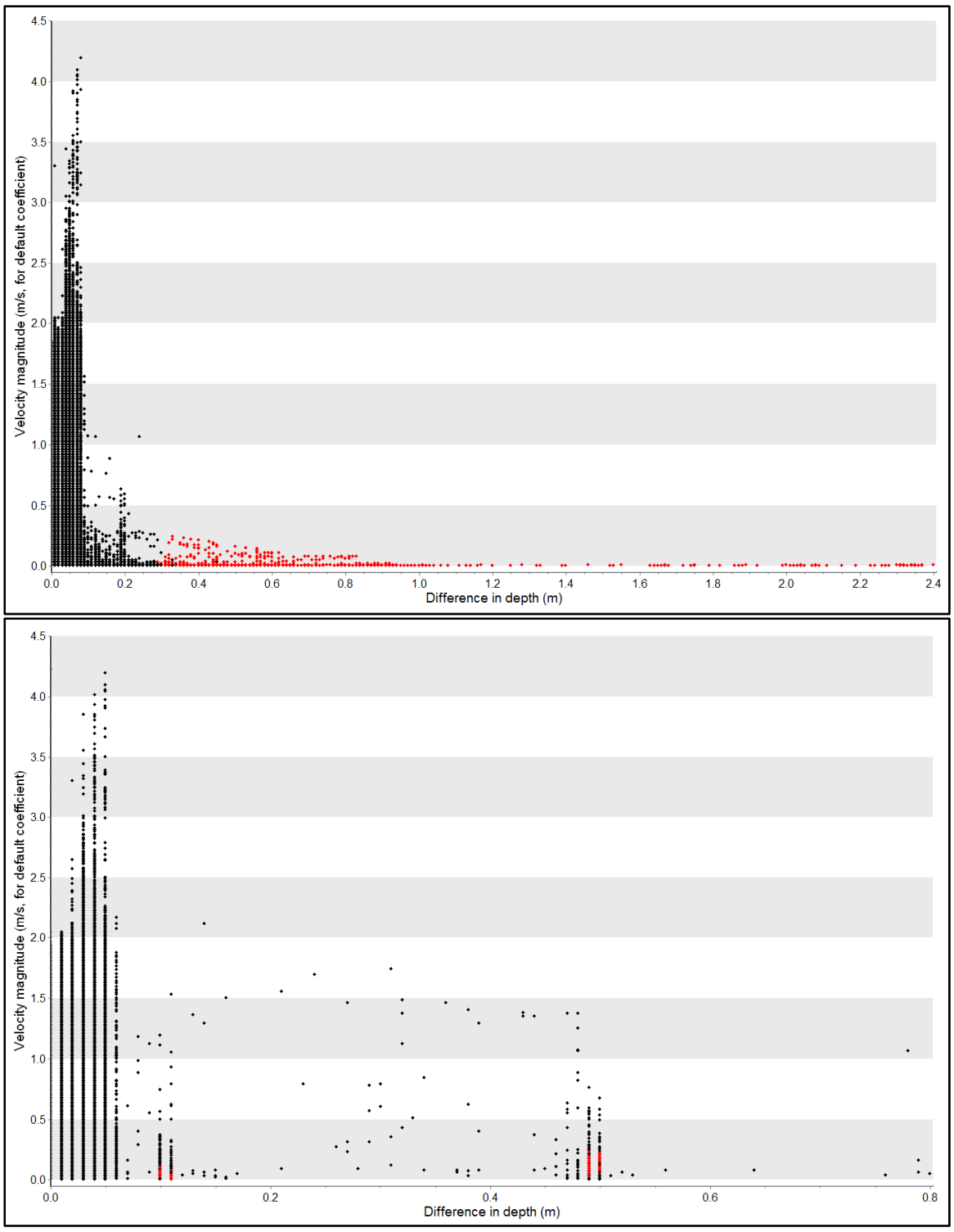


Figure 4.9. Comparison of velocity magnitude using default turbulence coefficient to difference in depth between the default coefficient and the minimum coefficient (above) and the maximum coefficient (below).

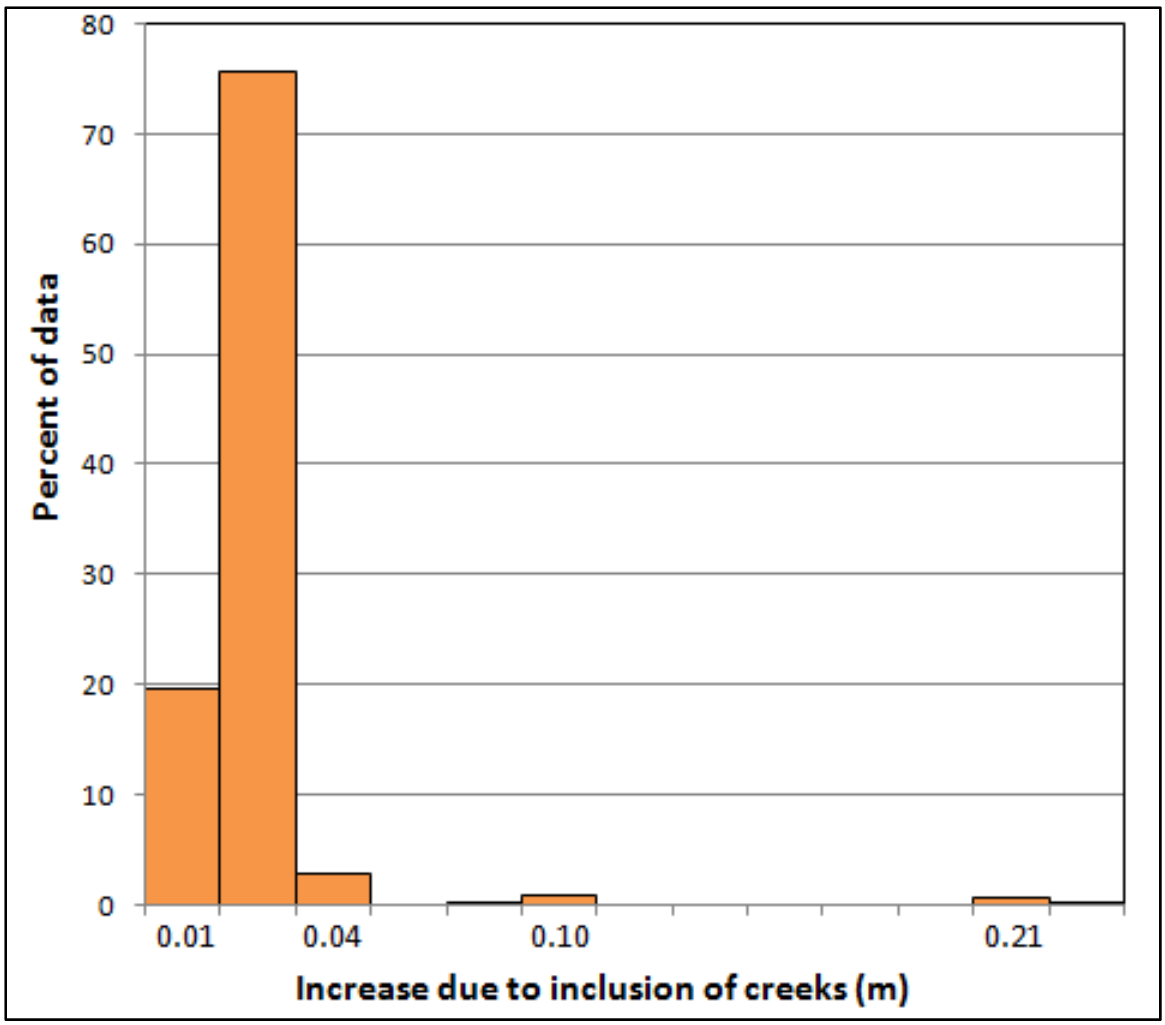


Figure 4.10. Effect of minor creeks on simulated water depth for an extreme flood event.

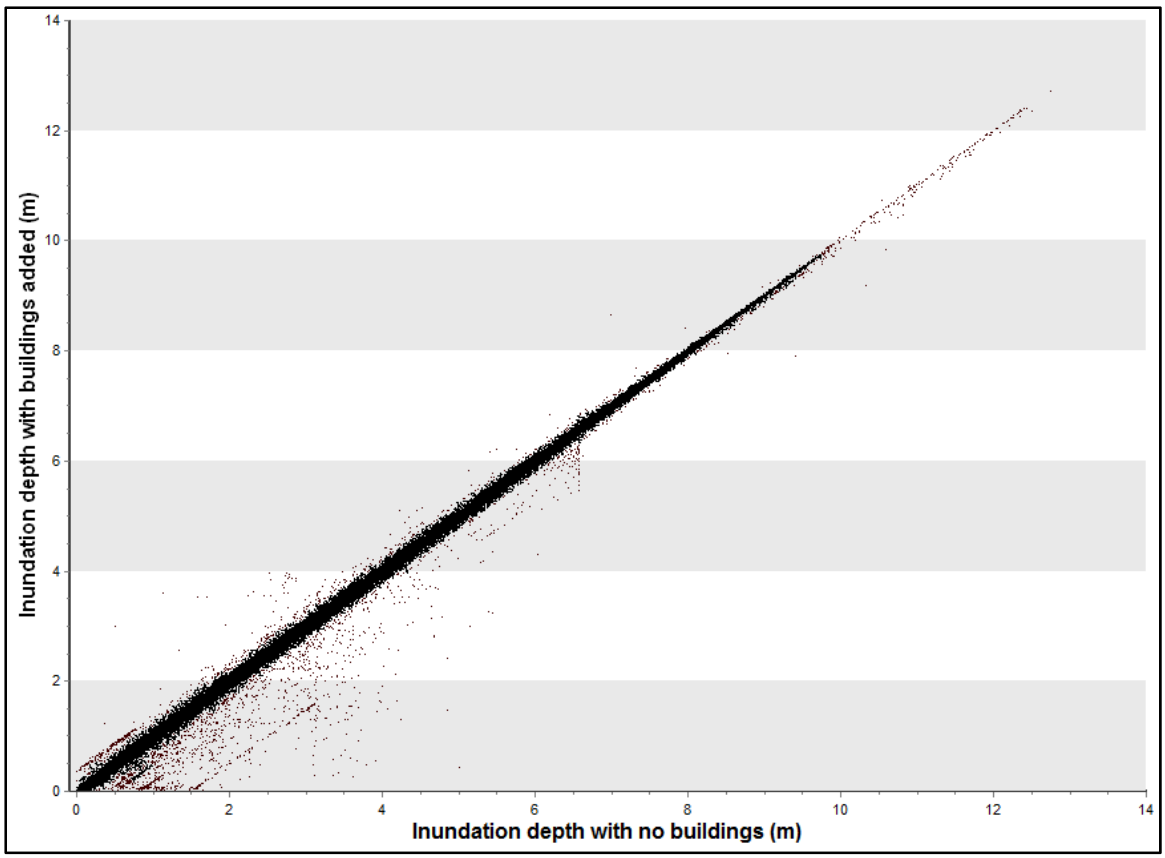


Figure 4.11. Effect of removing buildings from computational mesh.

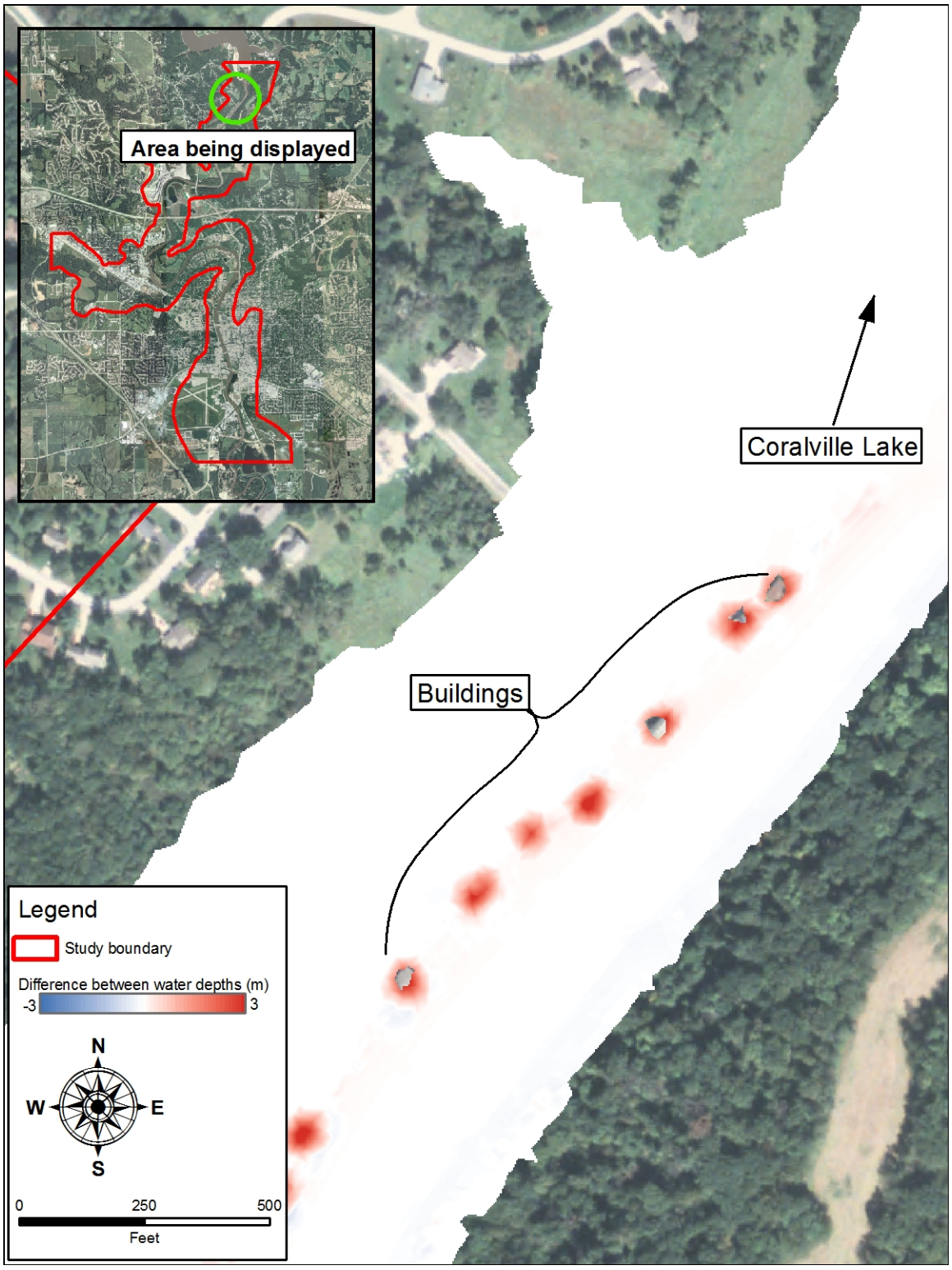


Figure 4.12. Simulated water depth using a DEM with extruded buildings subtracted from water depth with buildings removed from flow computations (difference in m).

Table 4.5. Over-prediction and standard deviation of 1D simulation, using 2D simulation results for comparison.

| Statistic | 1993 flood | 100-year flood | 500-year flood |
|---|---|---|---|
| Mean | -0.04 | 0.38 | -0.01 |
| Standard Deviation | 0.65 | 0.71 | 0.55 |

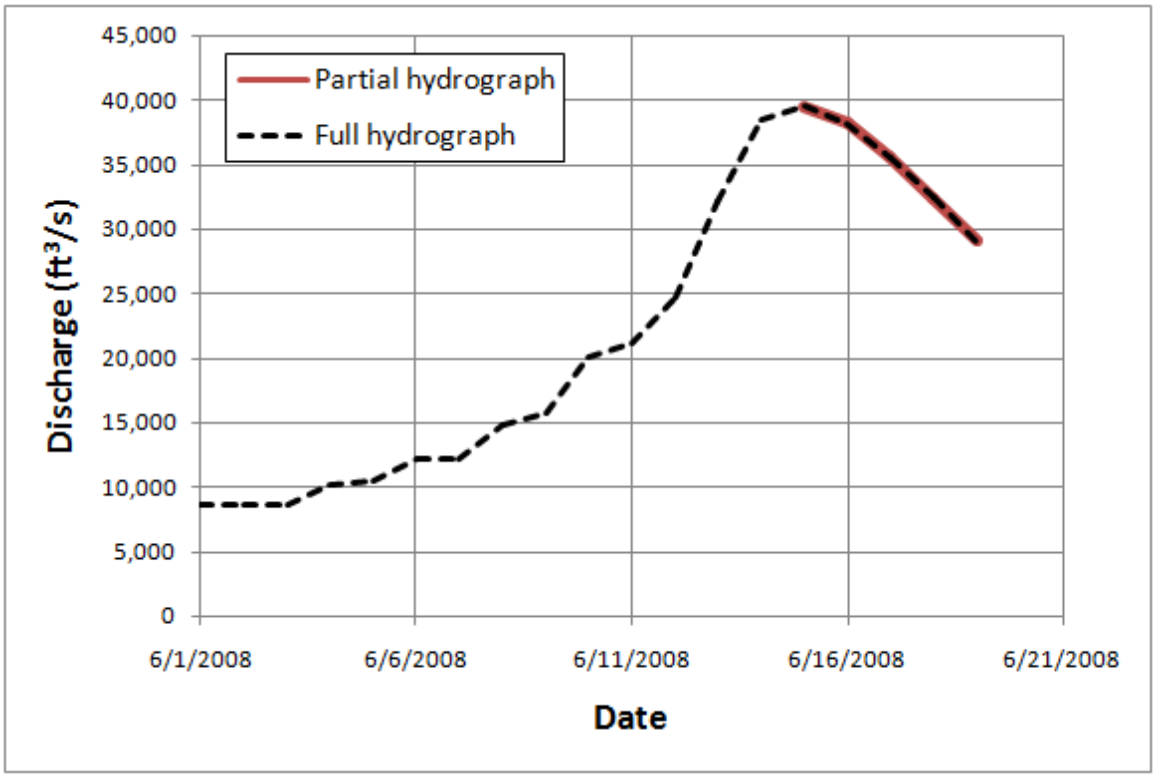


Figure 4.13. Unsteady hydrographs used in comparison to steady-state simulation

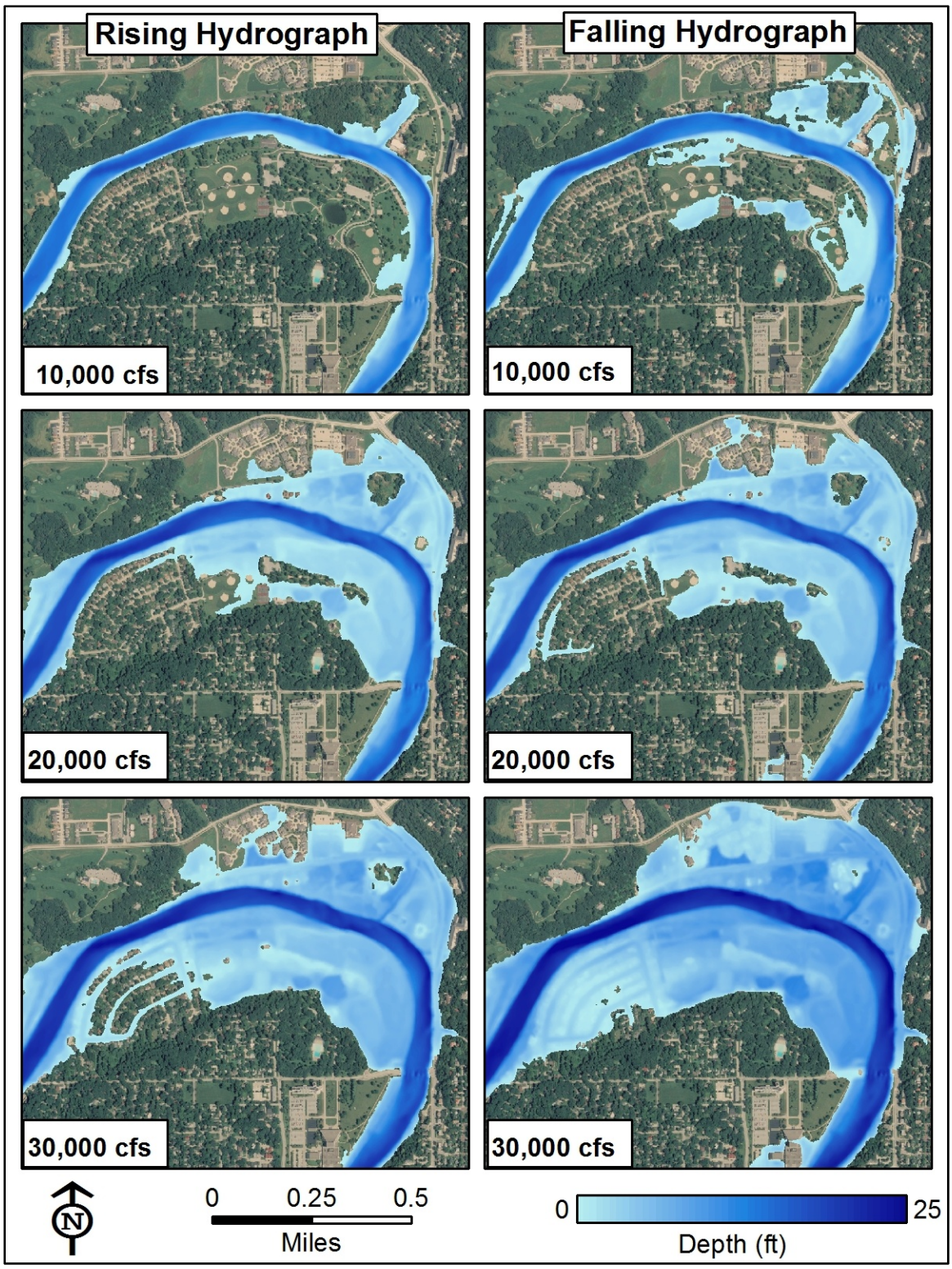


Figure 4.14. Effect of hysteresis in the vicinity of City Park.

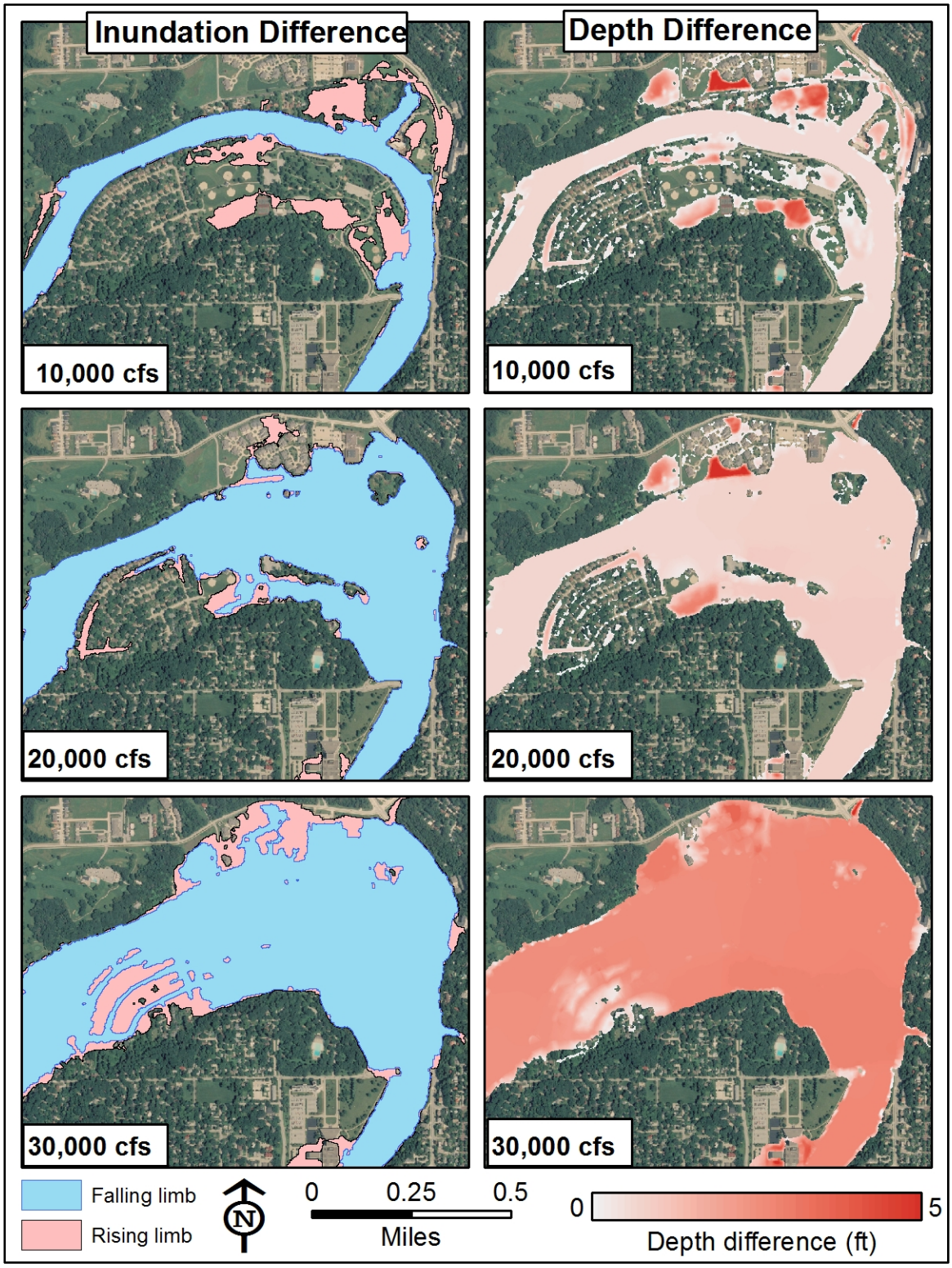


Figure 4.15. Differences in inundation extent and depth due to hysteresis.

# CHAPTER 5: CONCLUSIONS AND RECOMMENDATIONS

## 5.1 Summary

The study presents the development of a high-resolution hydrodynamic model of a 10-mile reach of the Iowa River corridor downstream of Coralville Lake. The numerical model represents the most accurate, precise, and highest-resolution representation of the Iowa River corridor to date, and is now the authoritative tool for flood preparation and mitigation. The numerical model will be used create a library of high-resolution maps along the Iowa River corridor, identifying the extent of flood inundation and magnitude of velocity associated with river flow and stage data reported by the National Weather Service. These maps will allow the local community agencies and citizens to better understand their individual flood risks, make more informed decisions about flood mitigation alternatives, and take appropriate actions to ensure safety and reduce damage during flood events. Maps of inundation depth and depth-averaged velocity magnitude will also help identify localized flood hazard zones where high depth or dangerous velocity is likely to occur.

To achieve this goal, a physically-based numerical code, namely SRH-2D, was utilized. SRH-2D requires bathymetric, topographic, hydrographic and bed shear-resistance data. In order to conduct hydrologic simulations, field measurements of bathymetry and topography were collected between July 2008 to October 2008 by the author and Ayres Associates. Hydrographic data were acquired from USGS and Ayres Associates. Bed shear resistance data were estimated from existing numerical modeling studies. The model was calibrated by modifying shear resistance values and comparing simulated WSE to discrete WSE measurements and data extracted from a continuous, high-resolution LiDAR data set. The calibrated model was validated using a high water mark survey conducted immediately after the 2008 flood peak.

The calibrated, validated model was used in multiple investigations and comparisons. Sensitivity to the turbulent eddy viscosity, effect of removing buildings

from the flow computations and effect of including minor creeks were investigated. Simulation results were compared to results from a 1D model of the same river reach to evaluate the benefits of the 2D model. Additionally, unsteady simulations of the flood hydrograph were compared to steady-state simulations to test the assumption that a steady-state simulation can approximate an unsteady hydraulic condition.

Findings of the study are as follows: (1) the run-time required for steady-state hydraulic conditions, using a well-equipped desktop computer, was found to be 62 hours for flood simulations and 48 hours for bankfull simulations; (2) the model adequately represents the water surface elevation in the main channel and floodplain; (3) the model is only sensitive to turbulent eddy viscosity for shallow depths (4) further investigation of the sensitivity to turbulent eddy viscosity should be performed; (5) lack of historic discharge data for minor creeks did not affect simulation accuracy; (6) reach scale simulation results are not affected by the removal of buildings from flow computations, and local inconsistencies were due to the methods used to represent buildings in the DEM; (7) The 1D model suffered from an inability to accurately predict inundation depth throughout the entire study area; (8) that high-resolution WSE data, such as LiDAR, may significantly improve numerical model calibration; (9) an unsteady hydrograph approximates flood hydrodynamics better than a steady-state simulation, but large computation time is not feasible for most investigations; (10) unsteady simulations should be performed with up-to-date hydrodynamic information to successfully mitigate future floods.

## 5.2 Future work

The study at hand provides a high-resolution representation of hydrodynamics in a floodplain corridor. Future modeling work should incorporate the methods of Mason et al. (2003) and use LiDAR data to derive spatiotemporally varying flow resistance values from vegetation height and density. The current investigation did not incorporate any model calibration based on velocity distribution. Future work should include field

measurements of velocity at multiple cross-sections within the model to improve calibration efforts. During extreme events, hydrodynamic interaction with urban storm sewers may become important. Recent work has used combined 2D overland flow and sewer models (Hsu, Chen and Chang 2000) and source/sink equations in 2D models (Gallegos, Schubert and Sanders 2009) to accurately simulate the effect of storm sewers during urban flood inundation. Comparing the current results to simulation results with storm sewer representation could quantify the effect of sewer surcharges. SRH-2D does not support internal boundary conditions, which could increase model fidelity in the vicinity of the two spillways. Future work, comparing the current results to simulation results with boundaries at the spillway defined by established empirical equations, would be beneficial. The author also intends to further investigate the differences in simulated inundation depth observed during the turbulent eddy viscosity sensitivity analysis to confirm or disprove the theory that narrow flow paths represented by few computational mesh elements were partially responsible for the difference in depth.

Additionally, higher-resolution topographic and bathymetric data would improve model fidelity: a multi-beam hydrographic survey and aerial LiDAR survey of the entire study reach at high and low stage, respectively, would remove the need for interpolation of bank line data by providing overlapping data sets. However, the admonishment of Hunter, et al. (2007) must be kept in mind: “producing assessments of flood risk at very fine spatial and temporal scales is not a panacea”. Investment in data collection and computational cost must be weighed against model resolution and fidelity.

# BIBLIOGRAPHY

Bates, P. D., M. D. Stewart, G. B. Siggers, C. N. Smitth, J. M. Hervouet, and R. H. J. Sellin. "Internal and External Validation of a Two-Dimensional Finite Element Code for River Flood Simulations." *Water and Maritime Engineering*, 1998: 127-141.

Bates, P.D., and A.P.J. De Roo. "A simple raster-based model for flood inundation simulation." *Journal of Hydrology*, 2000: 54-77.

Calder, B. R., and L. A. Mayer. "Automatic Processing of High-Rate, High-Density Multibeam Echosounder Data." *Geochemistry Geophysics and Geosystems.* Durham: American Geophysical Union, June 11, 2003.

Calenda, G., C. P. Mancini, and E. Volpi. "Distribution of the Extreme Peak Floods of the Tiber River from the XV Century." *Advances in Water Resources*, 2005: 615-625.

Chow, V.T. *Open-Channel Hydraulics.* New York: McGraw-Hill, 1959.

Cunge, J. A., F. M. Holly, and A. Verwey. *Practical Aspects of Computational River Hydraulics.* London: Pitman Publishing Limited, 1980.

Federal Emergency Management Agency. *Flood Insurance Study for Johnson County, Iowa and Incorporated Areas.* Washington D.C.: U.S. Department of Homeland Security, 2007.

Gallegos, Humberto A., Jochen E. Schubert, and Brett F. Sanders. "Two-Dimensional, High-Resolution Modeling of Urban Dam-Break Flooding: A Case Study of Baldwin Hills, California." *Advances in Water Resources*, 2009: 1323-1335.

Horritt, M. S. "Development of Physically Based Meshes for Two-Dimensional Models of Meandering Channel Flow." *International Journal for Numerical Methods in Engineering*, 2000: 2019-2037.

Hsu, M.H., S.H. Chen, and T.J. Chang. "Inundation simulation for urban drainage basin with storm sewer system." *Journal of Hydrology*, 2000: 21-37.

Huang, Motao, Guojun Zhai, Yongzhong Ouyang, and Yanchan Liu. "Data Fusion Technique for Multibeam Echosoundings." *Geo-spatial Information Science*, September 2002: 11-18.

Huang, Motao, Guojun Zhai, Yongzhong Ouyang, and Yanchun Liu. "Data Fusion Technique for Multibeam Echosoundings." *Geo-spatial Information Science*, September 2002: 11-18.

Hunter, Neil M., Paul D. Bates, Matthew S. Horritt, and Matthew D. Wilson. "Simple spatially-distrubuted models for predicting flood inundation: A review." *Geomorphology*, 2007: 208-225.

ISU GIS Facility. *Iowa Geographic Map Server.* 1999-2009. http://ortho.gis.iastate.edu/ (accessed 2008-2009).

Krajewski, Witold F., Larry Weber, Radoslaw Goska, and Bo Chen. *High Accuracy 3-D Inundation Information From LiDAR Data: A Pilot Study on the Iowa 2008 Flood.* Preliminary Report, Iowa City: Iowa Flood Center at the University of Iowa, 2009.

Lai, Yong G. *Two-Dimensional Depth-Averaged Flow Modeling with an Unstructured Hybrid Mesh.* Denver: Bureau of Reclamation Sedimentation and River Hydraulics Group, 2009.

Lai, Yong G., and Jennifer Bountry. *Numerical Modeling Study of Levee Setback Alternatives for Lower Dungeness River, Washington.* Project Report, Denver: U.S. Department of the Interior Bureau of Reclamation, 2007.

Mason, David C., David M. Cobby, Matthew S. Horritt, and Paul D. Bates. "Floodplain Friction Parameterization in Two-Dimensional River Flood Models Using Vegetation Heights Derived From Airborne Scanning Laser Altimetry." *Hydrological Processes*, 2003: 1711-1732.

Mignot, E., A. Paquier, and S. Haider. "Modeling floods in dense urban areas using 2D shallow water equations." *Journal of Hydrology*, 2006: 186-199.

Neal, Jeffrey C., Paul D. Bates, Timothy J. Fewtrell, Neil M. Hunter, Matthew D. Wilson, and Matthew S. Horritt. "Distributed Whole City Water Level Measurements from the Carlisle 2005 Urban Flood Event and Comparison with Hydraulic Model Simulations." *Journal of Hydrology*, 2009: 42-55.

Pappenberger, Florian, Patrick Matgen, Keith J. Beven, Jean-Baptiste Henry, Laurent Pfister, and Paul Fraipont. "Influence of Uncertain Boundary Conditions and Model Structure on Flood Inundation Predictions." *Advances in Water Resources*, 2006: 1430-1449.

Sauer, V. B., and R. W. Meyer. *Determination of Error in Individual Discharge Measurements.* Open-File Report, Norcross, Georgia: U.S. Geological Survey, 1992.

Schumann, Guy, et al. "High-Resolution 3-D Flood Information From Radar Imagery for Flood Hazard Management." *IEEE Transactions on Geoscience and Remote Sensing*, 2007: 1715-1725.

US Army Corp of Engineers. *Rivergages.com.* 2009. http://www2.mvr.usace.army.mil/WaterControl/new/layout.cfm (accessed 2008-2008).